



HAL
open science

Skull shape variation in extant pangolins (Pholidota: Manidae): allometric patterns and systematic implications

Sérgio Ferreira-Cardoso, Guillaume Billet, Philippe Gaubert, Frédéric Delsuc, Lionel Hautier

► To cite this version:

Sérgio Ferreira-Cardoso, Guillaume Billet, Philippe Gaubert, Frédéric Delsuc, Lionel Hautier. Skull shape variation in extant pangolins (Pholidota: Manidae): allometric patterns and systematic implications. *Zoological Journal of the Linnean Society*, 2019, 188, pp.255 - 275. 10.1093/zoolinnean/zlz096 . hal-02869913

HAL Id: hal-02869913

<https://sde.hal.science/hal-02869913>

Submitted on 16 Jun 2020

HAL is a multi-disciplinary open access archive for the deposit and dissemination of scientific research documents, whether they are published or not. The documents may come from teaching and research institutions in France or abroad, or from public or private research centers.

L'archive ouverte pluridisciplinaire **HAL**, est destinée au dépôt et à la diffusion de documents scientifiques de niveau recherche, publiés ou non, émanant des établissements d'enseignement et de recherche français ou étrangers, des laboratoires publics ou privés.

Skull shape variation in extant pangolins (Pholidota: Manidae): allometric patterns and systematic implications

SÉRGIO FERREIRA-CARDOSO^{1,*}, GUILLAUME BILLET^{2,*}, PHILIPPE GAUBERT^{3,4},
FRÉDÉRIC DELSUC¹ and LIONEL HAUTIER^{1,5}

¹*ISEM, Université de Montpellier, CNRS, IRD, EPHE, Montpellier, France*

²*Centre de Recherche en Paléontologie Paris (CR2P), UMR CNRS 7207, MNHN, CNRS, SU, Muséum National d'Histoire Naturelle, Paris, France*

³*Laboratoire Evolution et Diversité Biologique (EDB), Université Paul Sabatier, Toulouse, France*

⁴*CIIMAR/CIMAR, Centro Interdisciplinar de Investigação Marinha e Ambiental, Universidade do Porto, Porto, Portugal*

⁵*Mammal Section, Life Sciences, Vertebrate Division, The Natural History Museum, London, UK*

Received 22 February 2019; revised 17 July 2019; accepted for publication 13 August 2019

Pangolins are among the most endangered groups of mammals, comprising eight extant species delineated into three genera. Despite several studies dedicated to their skeletal anatomy, the potential taxonomic insight from cranial morphological variation in extant Pholidota is yet to be assessed with modern geometric morphometric methods. We present the first comprehensive study on the cranial morphology of extant pangolins and discuss its implications for the taxonomy and evolution of the group. We performed landmark-based morphometric analyses on 241 museum specimens to describe the variation in skull shape in seven of the eight extant species. Our analyses revealed genus- and species-level morphological discrimination, with Asian species (*Manis* spp.) being grouped together, whereas African pangolins present distinct skull shapes between small (*Phataginus* spp.) and large (*Smutsia* spp.) species. Analyses of allometry also identified a set of traits whose allometric trajectories distinguish Asian from African specimens. Finally, we uncovered intraspecific variation in skull shape in white-bellied pangolins (*Phataginus tricuspis*) that partly corroborates recent DNA-based differentiation among biogeographically distinct populations. Overall, our results shed light on the morphological diversity of the skull of these enigmatic myrmecophagous mammals and confirm the genus-level classification and cryptic diversity within the white-bellied pangolin revealed by molecular phylogenetics.

ADDITIONAL KEYWORDS: allometry – conservation – cryptic lineages – ontogeny – systematic.

INTRODUCTION

Extant pangolins [Pholidota (Weber, 1904) Manidae (Gray, 1821)] are currently the most heavily poached mammals in the world (Challender *et al.*, 2014; Zhou *et al.*, 2014). The increasing demand for pangolin scales in Chinese traditional medicine is driving this entire group to the brink of extinction. In that context, detailed morphological and genetic studies constitute a prerequisite to trace the geographical origin of seized specimens and may prove fruitful to delimitate new

and more effective conservation management units (von Helversen *et al.*, 2001; Hebert *et al.*, 2004; Bickford *et al.*, 2007; Moraes-Barros *et al.*, 2007; Galatius *et al.*, 2012; Hautier *et al.*, 2014; Sveegaard *et al.*, 2015; Gaubert *et al.*, 2016). The eight extant pangolin species are restricted to tropical and intertropical regions of sub-Saharan Africa and Southeast Asia (Gaubert, 2011; Gaudin *et al.*, 2019). They are classified in a single family (Manidae) within the order Pholidota, which is most closely related to carnivores within placental mammals (Murphy *et al.*, 2001a, b). Pangolins have evolved a set of highly distinctive morphological traits, such as toothless jaws and an

*Corresponding author. E-mail: sergio.ferreira-cardoso@umontpellier.fr

elongated rostrum, linked to their highly specialized diet of ants and termites (Ferreira-Cardoso *et al.*, 2019; Gaudin *et al.*, 2019). Despite this unique evolutionary history and their current protection status, pangolins are among the least studied placental mammals, with some aspects of their phenotypic variation (i.e. cranial shape) still being completely unexplored (Gaubert *et al.*, 2018).

The taxonomy of extant pangolins has been relatively unstable, varying from a single genus (*Manis* Linnaeus, 1758; Jentink, 1882; Emry, 1970) to six genera (Pocock, 1924). Based on both morphological and molecular phylogenetic studies, the four African species have been split into two genera (*Phataginus* Rafinesque, 1821 and *Smutsia* Gray, 1865), whereas the four Asian species remained in a single genus (*Manis*) (Gaudin *et al.*, 2009; Gaubert *et al.*, 2018). A recent molecular phylogeographical study also identified six cryptic lineages within the widely distributed white-bellied pangolin (*Phataginus tricuspis* Rafinesque, 1821), showing an unexpected intraspecific molecular divergence (Gaubert *et al.*, 2016). Likewise, several genetic clusters have been identified in the range of the Sunda pangolin (*Manis javanica* Desmarest, 1822), although their geographical delineation remains unclear (Zhang *et al.*, 2015; Nash *et al.*, 2018). Many aspects of inter- and intraspecific diversity of pangolins are still unexplored, and this newly described cryptic diversity has great potential to influence regional conservation policies and to identify the geographical origin of illegally trafficked specimens.

Geometric morphometrics has proved to be an efficient way to define the patterns of shape variation associated with species delimitation (interspecific taxonomy; e.g. Cardini & O'Higgins, 2004; Villemant *et al.*, 2007) and to unveil hidden morphological variation (intraspecific taxonomy; e.g. Hautier *et al.*, 2014, 2017; Miranda *et al.*, 2018). Such methods also enable us to understand the role of interactions between size and shape, with the variation in shape correlated with size (allometry) being one of the main factors contributing to the integrated evolution of cranial shape (Cardini & Polly, 2013; Klingenberg, 2013; Cardini, 2019). In mammals, ontogenetic and evolutionary allometry is mainly associated with elongation of the rostrum (Cardini & Polly, 2013; Cardini *et al.*, 2015). However, the variation in shape and size of the pangolin skull has never been described in detail or quantified formally, although the elongated, toothless snout constitutes one of the main characteristics of their skull. A precise characterization of the changes in shape associated with growth in pangolins should enable us to understand the extent to which allometry has contributed to the evolution of the skull.

Here, we applied geometric morphometric methods to study the variation in shape of the skull within and among the eight extant pangolin species, with the aim of assessing their current taxonomy and the recently identified molecular lineages. First, we examined the patterns of ontogenetic allometry in extant Pholidota using regression and trajectory analyses. Second, we explored the variation in cranial morphology among and within the three extant genera by performing regression, ordination and discriminant analyses. Finally, we investigated the variation in the shape of the skull in two wide-ranging species (*P. tricuspis* and *M. javanica*) in order to assess whether molecular-based cryptic lineages (Gaubert *et al.*, 2018; Nash *et al.*, 2018) differ in skull shape.

MATERIAL AND METHODS

BIOLOGICAL SAMPLING AND DATA COLLECTION

The material used in this study belongs to the collections of the Natural History Museum (BMNH) in London (UK), the Museum für Naturkunde (MfN) in Berlin (Germany), the Muséum National d'Histoire Naturelle (MNHN) in Paris (France), the Royal Museum for Central Africa (KMMA/RMAC) in Tervuren (Belgium), the American Museum of Natural History (AMNH) in New York (NY, USA) and the National Museum of Natural History (USNM) in Washington (DC, USA).

Our dataset is the result of the landmarking of 243 specimens from the eight extant species of pangolins (Fig. 1): *P. tricuspis* (Fig. 2; white-bellied pangolin, $N = 97$), *Phataginus tetradactyla* (Linnaeus, 1766) (black-bellied pangolin, $N = 23$), *Smutsia gigantea* (Illinger, 1815) (giant ground pangolin, $N = 16$), *Smutsia temminckii* (Smuts, 1832) (Cape pangolin, $N = 21$), *Manis crassicaudata* Geoffroy, 1803 (Indian pangolin, $N = 10$), *M. javanica* (Sunda pangolin, $N = 38$), *Manis pentadactyla* Linnaeus, 1758 (Chinese pangolin, $N = 36$) and *Manis culionensis* (de Elera, 1915) (Palawan pangolin, $N = 2$; Supporting Information, Appendix S1). The skull shape of the Palawan pangolin could not be assessed quantitatively owing to the low number of specimens available and the relatively large number of missing landmarks [a principal components analysis (PCA) including this species is provided in the Supporting Information, Fig. S1]. Taxa were identified based on a list of morphological criteria identified in the present study and in previously published works (Supporting Information, Appendix S2; Hatt *et al.*, 1934; Gaudin *et al.*, 2009, 2019). Different sizes of skulls were included to account for the change in shape during ontogeny. Given the absence of teeth in pangolins, the determination of age is not straightforward. For each species, juveniles were defined arbitrarily as those for which size (estimated by the centroid size; see below) fell

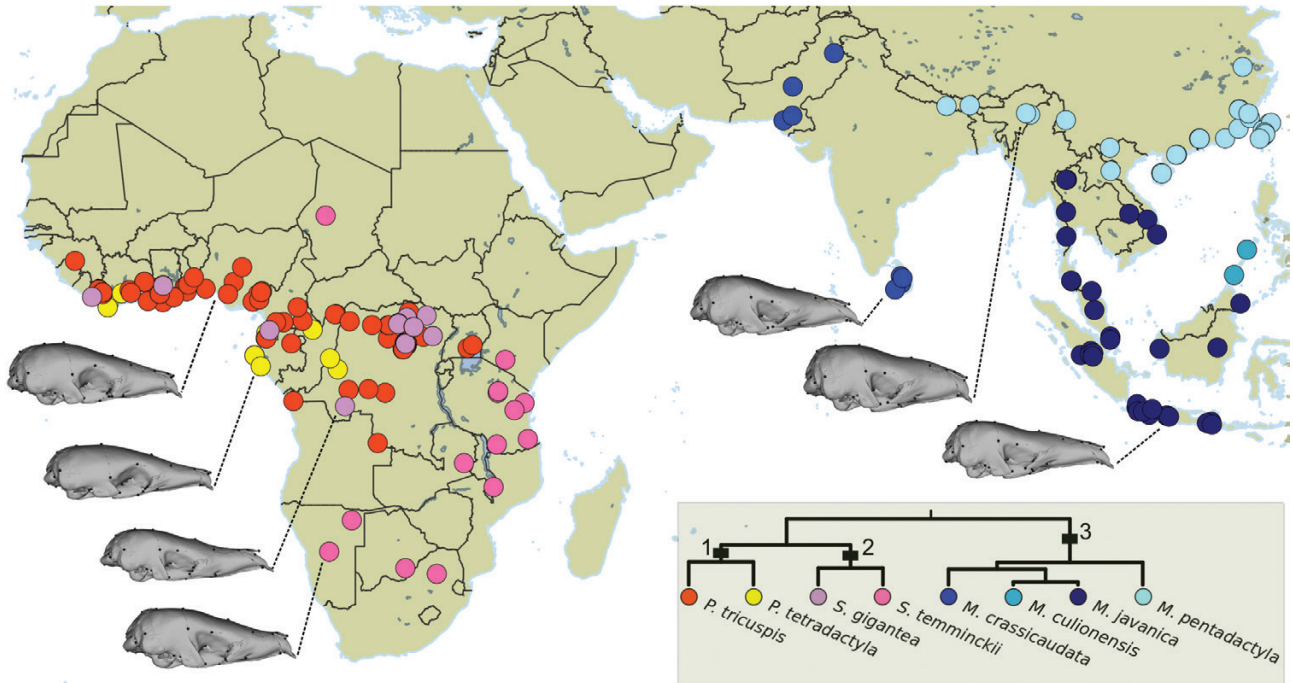


Figure 1. Geographical distribution of the sampled specimens ($N = 243$) belonging to eight species of pangolins. Mean shapes are illustrated for each species, except for *Manis culionensis*. The phylogenetic relationships used the branch lengths from Gaubert *et al.* (2018). 1, Phatagininae; 2, Smutsiinae; 3, Maniinae.

below the first quartile value (25% smallest specimens) for each species.

We placed 75 three-dimensional landmarks on pangolin skulls using a Revware MicroScribe M 3D digitizer (Fig. 3; Supporting Information, Table S1). Our selection of landmarks was based on previous works focused on mammalian taxa (e.g. Goswami, 2006; Hautier *et al.*, 2017). In a significant number of specimens, the premaxillae were absent, loosely attached or broken and could not be landmarked. In pangolins, the jugal bone is often absent. However, some *M. pentadactyla* specimens presented a complete zygomatic arch (see also Emry, 2004). In such cases, the landmarks 58/72 (zygomatic process of the maxillae) were hard to define accurately. They were therefore considered as missing and estimated a posteriori.

Thin plate spline interpolations (Gunz *et al.*, 2009) were computed to estimate missing landmarks for each group (e.g. species, cryptic lineages). This approach was implemented in the software package ‘geomorph’ v.3.5.0 (Adams *et al.*, 2017) in R (R Development Core Team, 2013). A generalized Procrustes analysis (Rohlf & Slice, 1999) was performed on all sets of landmarks. All specimens were scaled to centroid size, optimally translated and rotated using a least-squares criterion. The coordinates retrieved by the generalized Procrustes analysis represented the shape of the skull of each specimen. An ANOVA was performed

on a subset of our data for which sex determination was available ($N = 120$), in order to assess sexual dimorphism in skull shape.

ALLOMETRY IN EXTANT PANGOLINS

The study of allometry can focus on three different levels (Cheverud, 1982; Klingenberg, 2016). Morphological changes can be associated with phylogenetic differences in size (evolutionary allometry), variation in size within a single ontogenetic stage (static allometry) or variation in size attributable to individual growth within a single species (ontogenetic allometry; e.g. Foth *et al.*, 2016; Esquerré *et al.*, 2017; Gray *et al.*, 2019). Here, we quantified evolutionary allometry and considered three traits of ontogenetic allometric trajectories: direction (slope), magnitude (length) and intercept. These aspects were controlled/investigated with three different analyses.

First, a phylogenetic multivariate regression of the mean shape of adult specimens ($N = 173$) against log-centroid size was performed to assess evolutionary allometry. This analysis was performed with *procD.pgls* from ‘geomorph’ using a consensus phylogeny from Gaubert *et al.*, (2018). Then, we focused on ontogenetic allometry using interspecific ($N = 241$) and intraspecific datasets. The cryptic lineages dataset including *P. tricuspis* included only

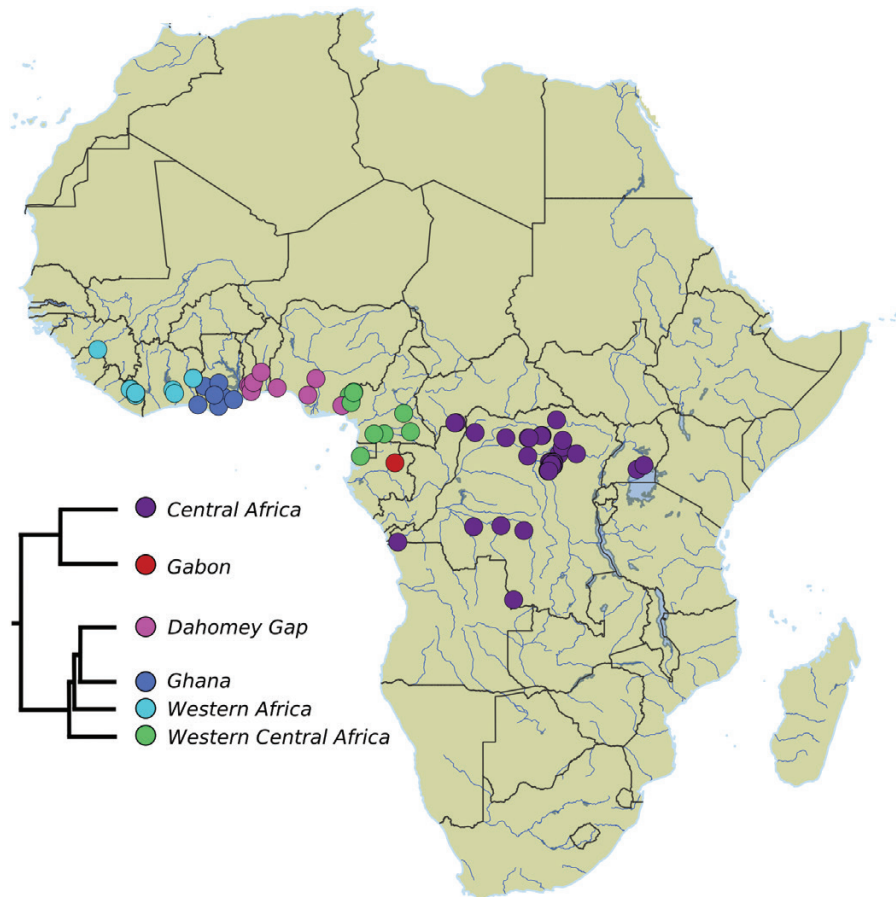


Figure 2. Map of Africa, with the locations of the sampled *Phataginus tricuspis* ($N = 96$) coloured according to the cryptic lineage (Gaubert *et al.*, 2016) to which they were attributed (right). The tree topology of the intraspecific affinities is based on Gaubert *et al.* (2018).

96 specimens (Fig. 2; KMMA 30808 was discarded owing to imprecise information on location). Details about the analysis of the *M. javanica* dataset can be found in the Supporting Information (Appendix S3). First, a multivariate regression was performed to assess covariation patterns between the logarithm of the centroid size and Procrustes-aligned coordinates (raw shapes) using *procD.lm* from ‘geomorph’. The hypothesis of parallel group slopes was assessed with a homogeneity of slopes (HOS) test. This test consists of an analysis of covariance (ANCOVA) to assess the influence of size, groups and the interaction of size and groups on skull shape. The HOS test includes pairwise comparisons between groups (species/cryptic lineages) to assess significant differences of both the direction (angles) and magnitude (amount of change in shape with size) of allometric trajectories. Significance was assessed with a residual randomization permutation procedure with 10 000 iterations. The HOS tests were performed with *advanced.procD.lm* from the package ‘geomorph’. The HOS tests were complemented by

graphical representations of allometric trajectories and skull shape deformations (Adams & Nistri, 2010; Esquerré *et al.*, 2017). We plotted the first principal component (PC1) of the predicted values of multivariate regression of shape on log-centroid size vs. log-centroid size regressions for each species. We then assessed the significance of differences between the intercepts using a Tukey means comparison, to test for changes in shape explained by species differences in the resulting morphospace. Thin plate splines were generated using the function *tps3D* from the R package ‘Morpho’ v.2.5.1 (Schlager, 2017) in order to characterize differences in shape between the smallest and the largest specimens for each species (ontogenetic allometry). We then visualized landmark displacement during ontogeny using the function *deformGrid3d* from the same package. A phenotypic trajectory analysis (PTA) was also performed as a complementary analysis to the HOS test (see Supporting Information, Appendix S3; Adams & Collyer, 2009; Collyer & Adams, 2013).

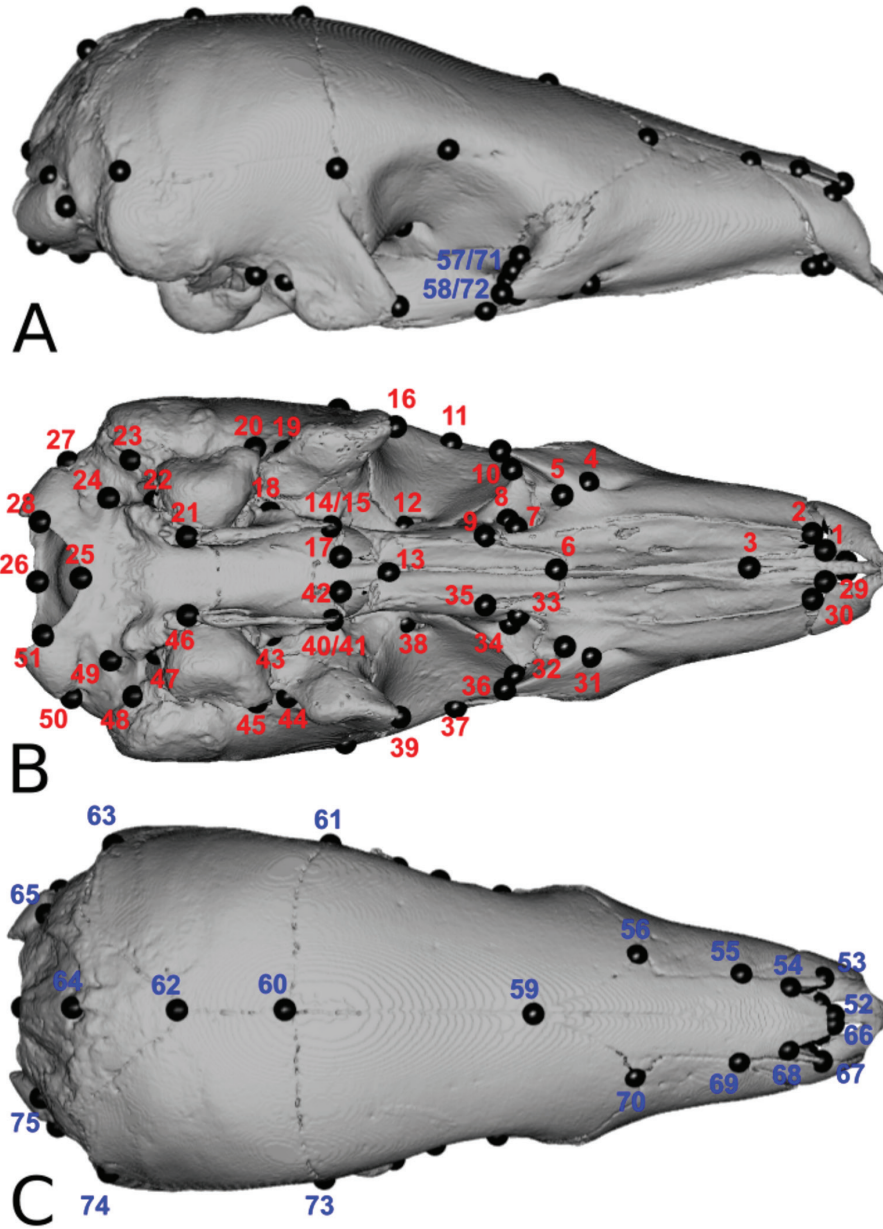


Figure 3. Landmarks digitized on the skull of *Phataginus tricuspis* (BMNH 34.6.2.92) in lateral (A), ventral (B) and dorsal (C) views. Red and blue numbers represent landmarks placed ventrally and dorsally, respectively.

Second, when the HOS test revealed parallel trajectories, we performed an additional analysis (overlap test) on multivariate shape data to test for overlap in ontogenetic allometric trajectories by comparing their differences with a set of 10 000 permutations (Piras *et al.*, 2011; Esquerré *et al.*, 2017). Intercepts were tested at $x = 5.125$, because we lacked fetuses and neonates of small size (close to $x = 0$), which could result in an incorrect estimate of minimum size

($x = 0$). The overlap test was performed only on the interspecific dataset.

Finally, if slopes were overlapping between species, a third analysis was performed to identify peramorphosis/paedomorphosis. This ‘heterochrony test’ enables the characterization of differences in skull shape at maximum size (Piras *et al.*, 2011; Esquerré *et al.*, 2017). Significance was assessed by comparing these differences with a set of 10 000

permutations. This test was performed only on the interspecific dataset.

VISUALIZATION OF SHAPE VARIATION AND STATISTICAL ANALYSIS

The variation of skull shapes was visualized using a PCA (Dryden & Mardia, 1993). Data were analysed without allometric correction in order to allow for a comparison of the results with morphological discrete characters used in phylogenetic analyses. Analyses with the allometry-corrected shapes for the interspecific and *P. tricuspis* datasets can be found in the Supporting Information (Appendix S3). Allometry-corrected shapes were obtained as the residuals of pooled within-group regressions. This method is used to obtain a common estimate for the allometry when comparing several groups (Sidlauskas et al., 2011; Benítez et al., 2013; Klingenberg, 2016). Pooled within-group regressions were performed in MorphoJ v1.06d (Klingenberg, 2011). For simplicity, when PCAs were performed on allometry-corrected shapes, axes were designated as PCres.

Interspecific variation in extant pangolins

A PCA was performed excluding specimens considered as juveniles ($N = 173$). A second PCA was performed on a dataset including juveniles and two specimens of *M. culionensis* ($N = 243$). We used a .ply surface of a micro-computed tomography-scanned *P. tricuspis* skull (BMNH 34.6.2.92), the species most closely resembling the mean shape. The surface was then deformed to the mean skull shape of Pholidota and used to visualize the variation in skull shape along the first three principal components (PCs). Triangular mesh warping via thin plate spline was performed with the package 'Morpho'.

A multivariate ANOVA was performed to assess whether skull shape differed between taxonomic groups. Pairwise comparisons between least-squares means were performed using *advanced.procD.lm*. If taxonomy had a significant effect on skull shape, a leave-one-out cross-validated linear discriminant analysis (LDA) was performed on a set of PCs explaining 90% of variance. The leave-one-out procedure allows evaluation of the accuracy with which unknown specimens can be identified (e.g. Evin et al., 2013). Linear discriminant analyses and post hoc classification methods were performed with the 'MASS' package (Venables & Ripley, 2002) in R.

Intraspecific variation in *P. tricuspis* and *M. javanica*

A second subset including only adult *P. tricuspis* specimens was analysed separately in order to

describe the intraspecific variation in skull shape ($N = 71$). We used the cryptic genetic lineages defined by Gaubert et al. (2016) to test the variation in skull shape linked to geographical distribution within *P. tricuspis*. Specimens were sorted according to six regions (Fig. 2): Western Africa (WAF), Ghana (GHA), Dahomey Gap (DHG), Western Central Africa (WCA), Central Africa (CAF) and Gabon (GAB). Skull shape difference tests and cross-validated LDA described in the previous paragraph were repeated on this dataset. If a posteriori attribution errors were consistently detected between two regions, these were merged, and the protocol was repeated with the new specimen sorting in order to test for its potential in assigning specimens with unknown geographical origin.

An equivalent protocol was applied to assess intraspecific variation in the skull of *M. javanica*. The geographical delimitation of cryptic lineages within this species is still uncertain (Zhang et al., 2015; Nash et al., 2018). These preliminary analyses can be found in the Supporting Information (Appendix S3).

The original landmark coordinates used in this study are provided in the Supporting Information (Appendix S1).

RESULTS

ALLOMETRY IN EXTANT PANGOLINS

A multivariate regression (Table 1) performed on raw shape variables revealed significant effects of log-transformed centroid size ($F_{1,227} = 103.59$, $P < 0.001$, $R^2 = 0.16$), species grouping ($F_{6,227} = 49.63$, $P < 0.001$) and of an interaction between centroid size and species grouping ($F_{6,227} = 1.35$, $P < 0.001$) on shape. When we accounted for phylogeny, the effect of size was marginally non-significant ($P = 0.09$), with evolutionary allometry explaining roughly one-third of skull shape variance ($R^2 = 0.27$; Supporting Information, Table S2). The non-significant P -value was probably attributable to the low number of species ($N = 7$). The HOS test

Table 1. ANOVA of shape (Procrustes coordinates) ~ log(centroid size)*species

	d.f.	R^2	F	P -value
Log(centroid size)	1	0.16	103.59	< 0.001*
Species	6	0.47	49.63	< 0.001*
Log(centroid size):species	6	0.01	1.35	< 0.001*
Residuals	227	0.37	–	–
Total	240	–	–	–

The randomized residual permutation procedure used 10 000 permutations.
*Significant P -value.

pairwise comparisons of ontogenetic allometric trajectories revealed small, significant differences (low z -values) between the slopes of *S. gigantea* compared with both *M. javanica* and *M. pentadactyla* (Supporting Information, Table S3). The remaining species did not present significantly different slope angles, which implied that allometric trajectories were parallel within each genus. The results for the PTA are presented in the Supporting Information (Appendix S3; Fig. S2; Tables S4 and S5).

The ontogenetic allometric trajectories overlapped in most species presenting parallel slopes except for *P. tricuspis* (Supporting Information, Table S6). The trajectory for *P. tetradactyla* overlapped with all the others except those of *M. javanica* and *P. tricuspis*. When comparison of the intercepts was performed considering shape predictions for $x = 0$, the ontogenetic allometric trajectories overlapped in all species (Supporting Information, Table S7). The heterochrony test showed that all species with overlapping trajectories presented heterochronic shifts with respect to each other (Supporting Information, Table S8).

The intercepts of the regressions of predicted values of shape against size (Fig. 4) were relatively distinct within *Phataginus* and *Manis*, whereas both *Smutsia* species presented overlapping trajectories, as revealed by the Tukey comparisons (Supporting

Information, Table S9). Considering the predicted shapes for minimum and maximum size resulting from the multivariate regression, the main size-related intraspecific morphological change was the increase in length of the rostrum (Figs 4, 5). Landmarks in the anterior part of the nasal and maxilla tended to be more anterodorsally positioned, and the nasal projected more posteriorly (e.g. Fig. 4, 5). The braincase was relatively lower in the adult, across all species, with the dorsal landmarks on the midline of the skull being more ventral when compared with their position in the juveniles (Fig. 5). Additionally, the landmarks placed on the zygomatic process of the maxilla and associated structures (Fig. 3; landmarks 10, 57 and 58) showed a tendency to project more posteriorly in larger specimens (Fig. 5A–D). In contrast, *S. temminckii* showed no allometric growth of the posterior projection of the zygomatic processes (Fig. 5E). In contrast, this species presented the most significant change in the anterior projection of the zygomatic process of the squamosal, with this structure being noticeably less projected in smaller specimens (Fig. 5E).

INTERSPECIFIC VARIATION OF THE SKULL SHAPE IN EXTANT PANGOLINS

A Procrustes ANOVA revealed that both sex ($F_{1,105} = 1.80$, $P = 0.085$; $F_{1,106} = 2.03$, $P = 0.057$) and

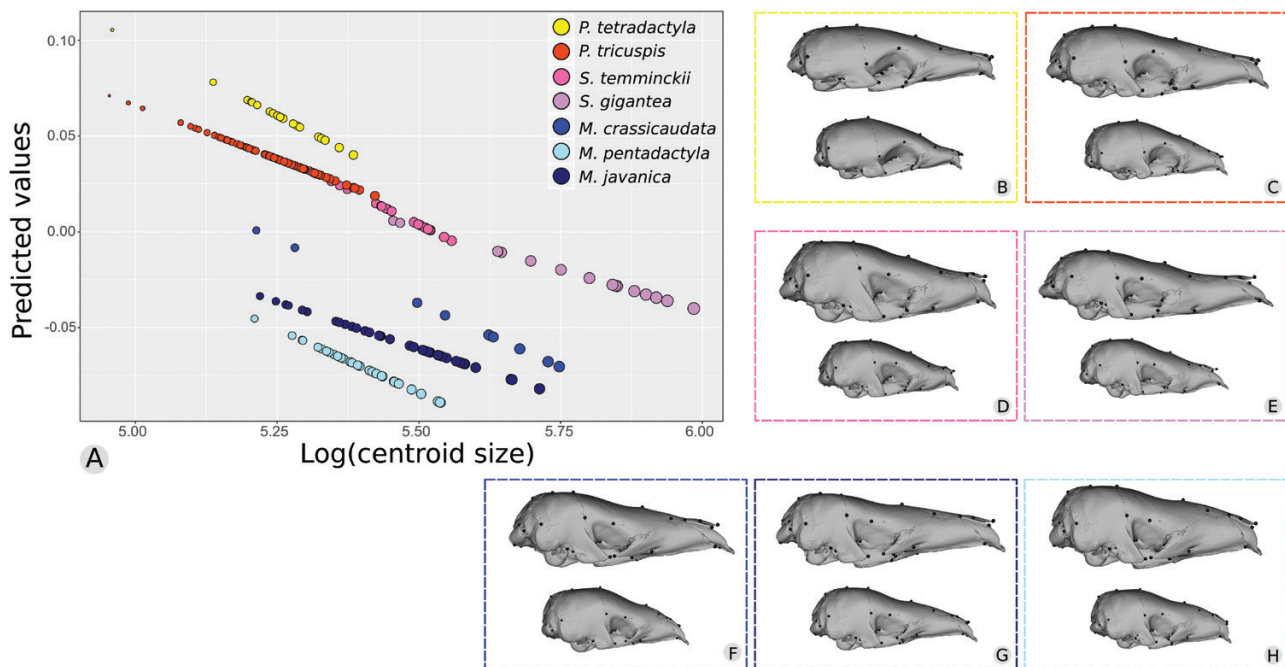


Figure 4. Allometric trajectories among seven pangolin species ($N = 241$). A, the x -axis values are the log-transformed centroid sizes for each specimen; the y -axis values are the principal component 1 of the predicted values of a multivariate regression of shape on size. B–H, deformed meshes for the maximum (top) and minimum (bottom) shapes predicted from a multivariate Procrustes regression for each species are presented.

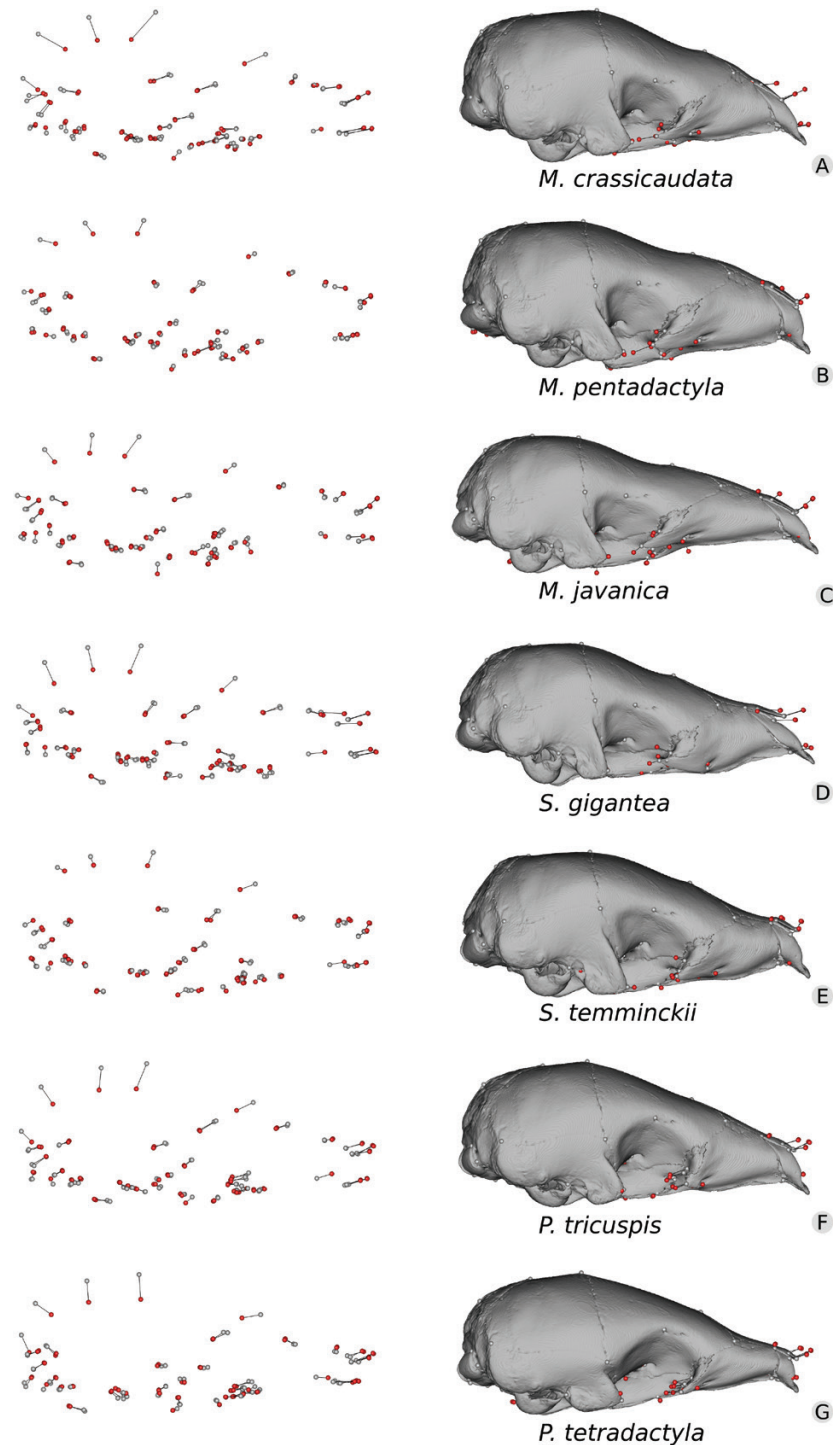


Figure 5. Mapping of ontogenetic variation in shape in seven pangolin species. A, *Manis crassicaudata*. B, *Manis pentadactyla*. C, *Manis javanica*. D, *Smutsia gigantea*. E, *Smutsia temminckii*. F, *Phataginus tricuspis*. G, *Phataginus tetradactyla*. Grey dots represent relative Procrustes coordinates positions in the juvenile (minimum-sized specimen), and red dots represent coordinates for the adult (maximum-sized specimen). Deformed meshes corresponding to juveniles were superimposed with the three-dimensional Procrustes coordinates.

the interaction between sex and species grouping ($F_{6,105} = 0.89, P = 0.656$; $F_{6,106} = 1.07, P = 0.332$) did not significantly influence shape, with and without considering size as a covariate in the model, respectively ($N = 120$; [Supporting Information, Table S10](#)). The Procrustes ANOVA performed with the adult dataset revealed a significant effect of species on skull shape ($F_{6,166} = 45.02, P < 0.001$; [Table 2](#)). Pairwise comparisons showed that all species presented significantly different skull shapes ([Supporting Information, Table S11](#)). The variation in skull shape was visualized using a PCA performed on the raw shape variables of the seven pangolin species ([Fig. 6](#)). The results of a PCA including juveniles and *M. culionensis* ([Supporting Information, Fig. S1](#)) and a full analysis of allometry-corrected skull shape are presented in the [Supporting Information \(Appendix S3; Fig. S3; Tables S12, S13\)](#). Despite the non-parallel slopes, the variance explained by the interaction between size and species was relatively low ([Table 1](#)), allowing us to use the residuals of a multivariate regression of shape on size as allometry-corrected shapes.

Linear regressions performed on the first 30 PCs (90%) showed that size was significantly correlated with PCs 1–4 and PC7 ([Supporting Information, Table S14](#)). Size-related morphological changes captured by PC1 appeared to be associated mainly with evolutionary allometry, whereas change in shape along PC2 recovered differences related to ontogenetic allometry. The first two PCs explained 49.59% of the total variance (33.95 and 15.64%, respectively).

Principal component 1 was positively correlated with a high and wide rostrum, a nasofrontal inflation associated with an orbital constriction, posteriorly projected zygomatic processes of the maxillary and a high and wide braincase, with dorsal squamosal-parietal-frontal junctions. African specimens tended to display mostly negative PC1 scores, whereas the Asian clade exhibited positive PC1 scores ([Fig. 6A, B](#)). The sole exception was the African *S. gigantea*, which presented positive PC1 values and grouped with Asian specimens ([Fig. 6](#)). Principal component 1 also separated the two African genera (*Phataginus* presented the most

negative scores). Juvenile specimens of Asian species were characterized by less positive PC1 values, plotting closer to African pangolins (see ‘Results: allometry within extant pangolins’; [Supporting Information, Fig. S1](#)).

Principal component 2 was positively correlated with a long rostrum, a long posterior projection of the premaxilla on the midline, an anterolaterally projecting zygomatic process of the squamosal and a braincase with a pseudorectangular shape in dorsal view ([Fig. 6](#)). Principal component 2 separated the three species of *Manis* and the two *Smutsia*. *Smutsia temminckii* and *M. pentadactyla* scored the lowest PC2 average values, whereas *M. javanica* scored the highest. *Phataginus* spp., *S. gigantea* and *M. crassicaudata* presented PC2 scores ranging in between the two groups.

Principal component 3 scores were positively correlated with the anterior projection of the anterior flanges of the frontal, a wide and long palatine, a long infraorbital canal, an anteroposteriorly elongated dorsal edge of the zygomatic processes of the squamosal and posteriorly projected pterygoid hamuli ([Fig. 6B](#)). This axis separated species within *Phataginus* and *Smutsia*. *Phataginus tetradactyla* scored extremely positive PC3 values, whereas *S. gigantea* scored the most negative PC3. The three *Manis* species and *S. temminckii* presented values slightly above zero, on average, and *P. tricuspis* showed mostly negative values, but not as negative as *S. gigantea* ([Fig. 6B](#)).

An LDA was performed to take 90% of the variance into account (first 30 PCs). Linear discriminant analysis group a posteriori probabilities retrieved 100% accuracy for species attribution ([Supplemental Information, Appendix S4](#)). Specimens were grouped by species and were well discriminated on linear discriminants 1 and 2 (LD1, 54.0%; LD2, 15.6%; [Fig. 6C, D](#)). Asian pangolin skulls presented negative LD1 values, whereas African pangolins scored both negative (*Smutsia*) and extremely positive values (*Phataginus*; [Fig. 6C, D](#)). The three species of Maninae Gray, 1821 resembled each other the most, being discriminated only by LD2. Within the African clade, LD2 discriminated the two *Phataginus* species (*P. tetradactyla* showed the highest

Table 2. ANOVA of shape ~ taxa/geographical groups of adult specimens of the interspecific and *Phataginus tricuspis* datasets

Datasets	<i>N</i> taxa/geo	<i>N</i>	d.f.	<i>R</i> ²	<i>F</i>	<i>P</i> -value
Interspecific	7	173	166	0.62	45.02	< 0.001*
<i>P. tricuspis</i> (Gaubert et al., 2016)	6	70	65	0.16	3.12	< 0.001*
<i>P. tricuspis</i> (geographical groups)	3	70	67	0.11	4.23	< 0.001*

The randomized residual permutation procedure used 10 000 permutations. Significant *P*-values indicate differences between skull shapes of taxa/geographical groups.

Abbreviation: *N* taxa/geo, number of taxa or geographical groups used as factors.

*Significant *P*-value.

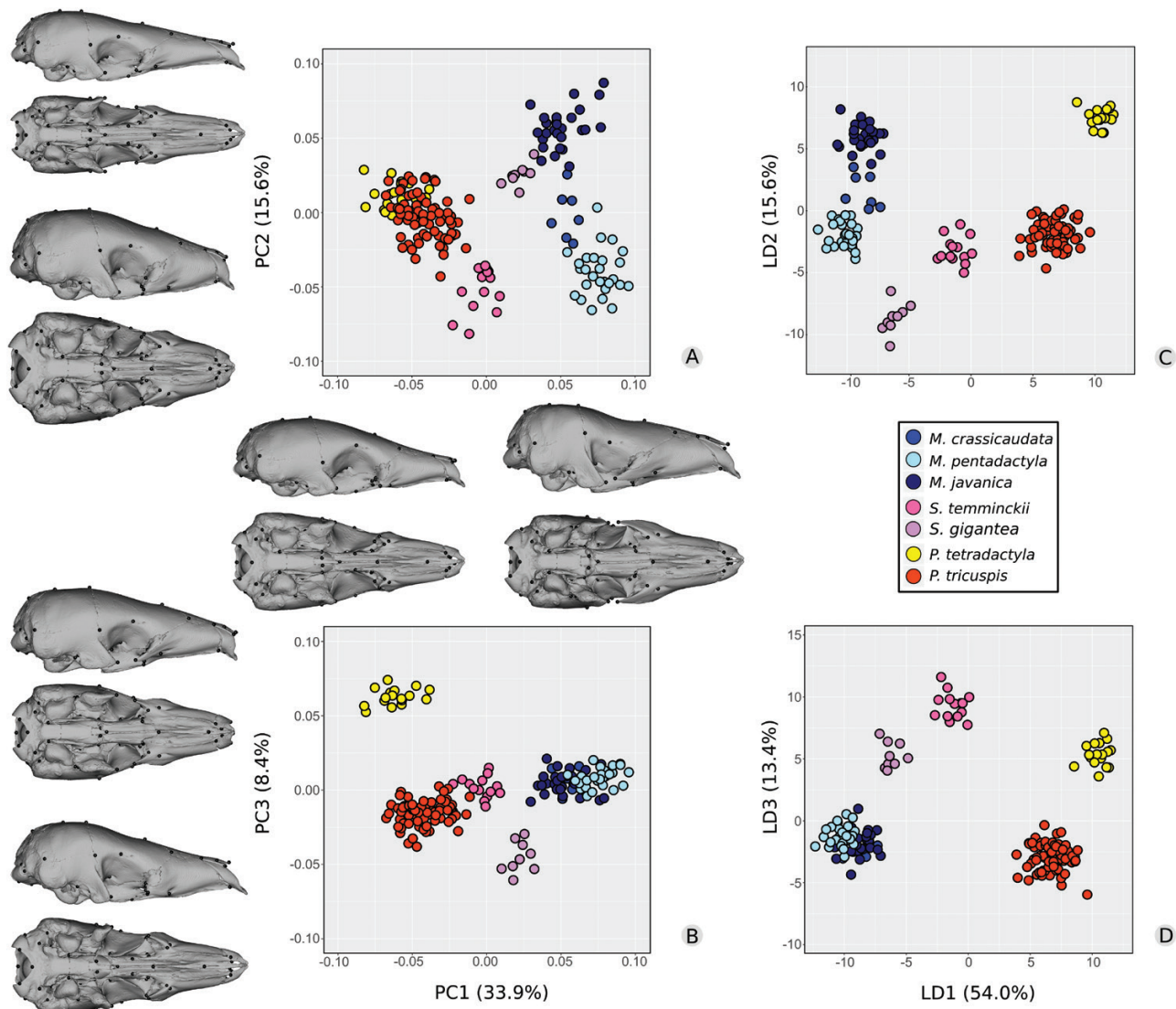


Figure 6. Principal components (A, PC1 vs. PC2; B, PC1 vs. PC3) and linear discriminant analyses (C, LD1 vs. LD2; D, LD1 vs. LD3) with associated variation in shape for crania of seven pangolin species ($N = 173$).

LD2 values). *Smutsia temminckii* and *S. gigantea* were well discriminated by LD1. *Smutsia* spp. showed the highest LD3 values.

The analyses on the allometry-corrected shapes revealed some differences that are discussed in detail in the [Supporting information \(Fig. S3; Tables S12 and S13\)](#).

INTRASPECIFIC VARIATION OF THE SKULL SHAPE IN EXTANT PANGOLINS

Intraspecific variation in P. tricuspis

A multivariate regression revealed that log-transformed centroid size ($F_{1,84} = 11.56$, $P < 0.001$) and geographical distribution (cryptic lineages; $F_{4,84} = 3.71$,

$P < 0.001$) had a highly significant effect on the cranial shape ([Table 3](#)). It also retrieved a significant effect of the interaction between size and geographical distribution ($F_{4,84} = 1.11$, $P = 0.001$). However, the pairwise matrix effect sizes were relatively small, and corresponding P -values were not significant. Therefore, all cryptic lineages presented parallel allometric trajectories ([Supporting Information, Fig. S4; Table S15](#)). A Procrustes ANOVA revealed that cryptic lineages presented different skull shapes ($F_{4,65} = 3.12$, $P < 0.001$; [Table 2](#)). Pairwise comparisons showed that all tested cryptic lineages presented significantly different skull shapes except for Ghana and Western Africa ([Supporting Information, Table S16](#)) Gabon was not tested owing to lack of replicates.

Table 3. ANOVA of shape (Procrustes coordinates) ~ log(centroid size)**Phataginus tricuspis* cryptic lineages ($N = 96$)

	d.f.	R^2	F	P -value
Log(centroid size)	1	0.10	11.56	< 0.001*
Cryptic lineages	5	0.15	3.71	< 0.001*
Log(centroid size):cryptic lineages	4	0.04	1.11	0.001*
Residuals	85	0.71	–	–
Total	95	–	–	–

The randomized residual permutation procedure used 10 000 permutations.

*Significant P -value.

Principal component 1 explained 12.8% of the variance of cranial shape within *P. tricuspis* and was positively correlated with a larger skull height and width, an anteroposteriorly short orbit, large tympanic bullae and a relatively round occipital region. Specimens from Central Africa mostly scored negative PC1 values (Fig. 7A, B). On average, specimens from WAF and GHA presented the most positive PC1 scores. The Western Central African cluster also presented mostly positive PC1 scores, whereas specimens from the Dahomey Gap presented a wide range of PC1 scores, varying from negative to positive values. The only specimen from Gabon scored negative PC1 values, plotting near the CAF morphospace.

Principal component 2 explained 9.7% of the variance and was positively correlated with a shorter palate with short maxillary projections, anteriorly projecting squamosal roots and shorter tympanic bullae well separated from the postglenoid foramina. Although specimens from CAF had a wide distribution along PC2, WCA, WAF and GHA presented a much narrower range of PC2 scores in the middle of the distribution. On average, DHG presented the most negative PC2 values.

Principal component 3 explained 6.4% of the variance (Fig. 7B) and did not segregate specimens according to geographical origin.

The LDA performed on the first 34 PCs (90% variance) discriminated WAF–GHA, DHG and CAF–WCA cryptic lineages, along LD1 (59.1%) (Fig. 7C). Western Africa–Ghana presented the most positive LD1 values, whereas CAF–WCA specimens presented mostly negative LD1 values (Fig. 7C, D). Specimens from DHG presented intermediate positive LD1 values. LD2 (23.7%) discriminated DHG skulls (negative values) from all other cryptic lineage specimens (Fig. 7C). LD3 (13.0%) discriminated the WCA specimens (most positive values) from the remaining lineages (Fig. 7D). Group a posteriori probabilities retrieved a 75.4% attribution accuracy

(see Supporting Information, Appendix S4). The vast majority of incorrect attributions were found in the major divisions WAF–GHA and CAF–WCA. Based on this result, we performed an additional LDA with a priori attributions of WAF–GHA specimens to a western group (WES) and CAF–WCA specimens to an eastern group (CEN), while keeping DHG as a separate group (Fig. 8). Group a posteriori probabilities of the LDA of the three groups shows an attribution accuracy of 95.7% (see Supporting Information, Appendix S4).

The additional LDA discriminated CEN from WES and DHG groups along LD1 (73.3%). LD2 (26.7%) discriminated CEN and WES from DHG groups. We tested the statistical significance of the intraspecific variation in the three groups identified above. A Procrustes ANOVA revealed a significant effect of the division of *P. tricuspis* into three morphological groups, WES, DHG and CEN ($F_{2,67} = 4.23$, $P < 0.001$; Table 2). Pairwise comparisons showed that all groups presented significantly different skull shapes (Supporting Information, Table S17). We calculated the mean shapes for each group (Supporting Information, Fig. S5). The WES skulls presented the shortest and widest rostrum, a relatively elongated infraorbital canal and the longest zygomatic process of the maxillary. The DHG skulls presented the widest nasals posteriorly, the most posterior projections of the maxilla into the palatine and the most posterior ventral margin of the foramen magnum. Skulls from the CEN region were characterized by the narrowest rostra, the smallest tympanic bullae and the most anterior petrosal–squamosal–exoccipital intersection.

The analyses on the allometry-corrected shapes revealed similar results (Supporting Information, Appendix S3; Fig. S6; Tables S12, S18, and S19).

Intraspecific variation in M. javanica

The analyses on the *M. javanica* dataset showed that differences in shape were solely explained by differences in size (Supporting Information, Figs S7, S8; Tables S12 and S20).

DISCUSSION

SIZE INFLUENCES SKULL SHAPE IN EXTANT PANGOLINS

Size explained a significant part of the total variation in skull shape among species within the Pholidota (evolutionary allometry; Table 1; Fig. 4; Supporting Information, Fig. S2; Table S2). The HOS and PTA tests showed that the directions of ontogenetic trajectories were conserved among pangolins, with only *M. javanica* and *M. pentadactyla* differing significantly from *S. gigantea* (HOS) and

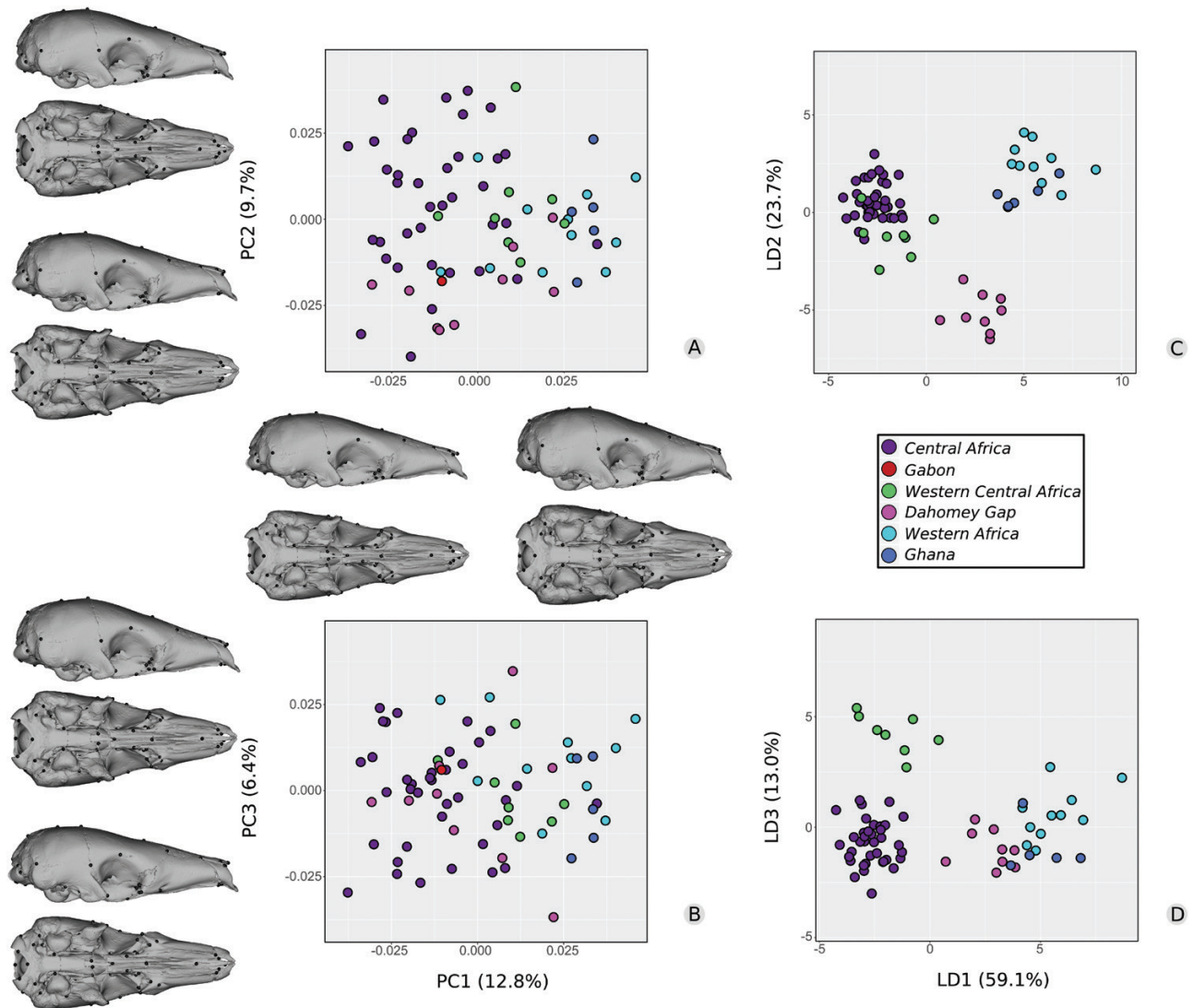


Figure 7. Principal components (A, PC1 vs. PC2; B, PC1 vs. PC3) and linear discriminant analyses (C, LD1 vs. LD2; D, LD1 vs. LD3) with associated variation in shape for crania of six cryptic lineages of *Phataginus tricuspis* ($N = 71$; Gaubert *et al.*, 2016).

P. tricuspis (PTA; Supporting Information, Tables S4 and S5). Ontogenetic trajectory angles did not differ within clades, which is consistent with observations that intraspecific (ontogenetic and/or static) allometric trajectories tend to differ as species divergence time increases (Voje *et al.*, 2014; Esquerré *et al.*, 2017).

Significant differences between the intercepts of multivariate regressions (overlap test) were found only between *P. tricuspis* and all other species and between *P. tetradactyla* and *M. javanica*. With the exception of the difference in intercept between the two *Phataginus* species, significant *P*-values were relatively close to 0.05 (i.e. same order of magnitude). This indicates that allometric trajectories are still relatively preserved across the Pholidota and

suggests that cranial morphology is similar in early developmental stages. The heterochrony test showed that more than half of the pairwise comparisons performed (12 out of 19) revealed heterochronic changes. In fact, when the overlap test was performed taking size = 0 as reference, heterochrony was detected for all 19 comparisons (Supporting Information, Tables S6 and S7). This could suggest a major pattern of heterochrony driving the differentiation between the Asian and African clades, the first being putatively peramorphic by presenting longer rostra and longer zygomatic processes of the maxilla (traits associated with the PC1 of the predicted values; Figs 4, 5). However, given the absence of fetuses in our analyses, predictions of shape at minimum size ($x = 0$)

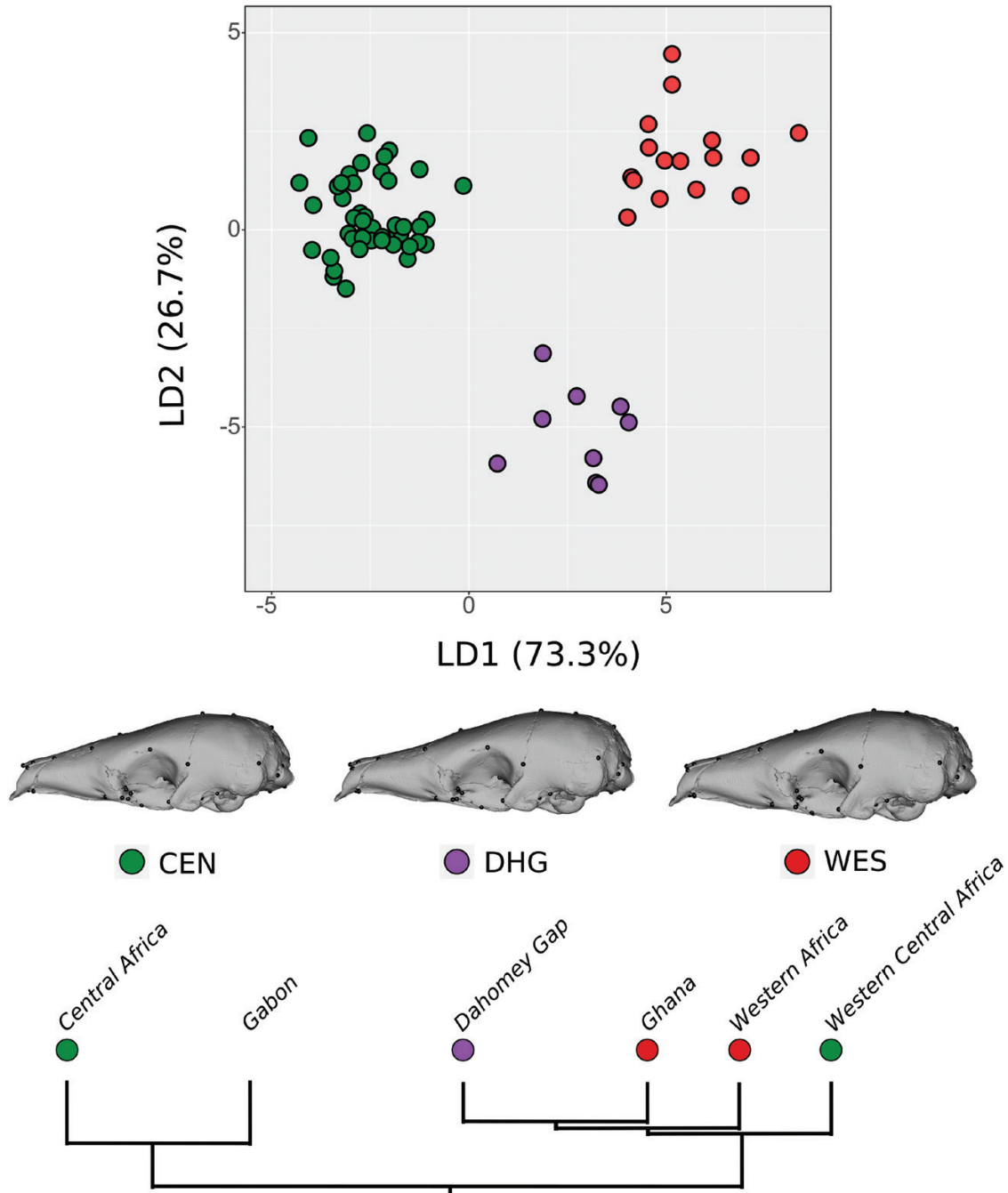


Figure 8. Linear discriminant analysis of the *Phataginus tricuspis* sample ($N = 70$) divided into three management units. Consensus shapes (mean shapes) of the proposed management units in lateral view. A, Central African region (CEN). B, Dahomey Gap region (DHG). C, western African region. Black dots are landmark positions.

should be considered with caution. Additionally, the heterogeneity of sampling between species might have influenced the significance of the overlap test, given that the largest differences between intercepts were not necessarily significant (Supporting Information, Table S6). The generally low P -values from the overlap test ($P < 0.23$) might reflect substantial differences

in the intercepts, despite the non-significance yielded (Amrhein *et al.*, 2019).

Moreover, African and Asian clades clearly presented non-overlapping ontogenetic allometric trajectories for traits correlated with PC1 of the predicted values of multivariate regression of shape on size (Fig. 4), with African species sharing a higher intercept relative

to Asian ones. We interpret this size–shape space as a good representation of the evolutionary allometry. Considering that parameters of modelled growth trajectories can be used efficiently as continuous characters in phylogenies (Bardin *et al.*, 2017), these different intercept values could theoretically constitute a valuable character to distinguish members of the Asian and African clades. In fact, they corroborate previous morphology- and DNA-based results (Gaubert *et al.*, 2018) that described a split of the extant Manidae into two continental clades. The differences in the ontogenetic allometric patterns between the two size–shape spaces (multivariate vs. PC1 of the predicted values) might also suggest strong cranial modularity (i.e. rostrum module; Goswami, 2006). Cranial modules evolve semi-independently, and allometric patterns detected for highly integrated modules might differ from the overall pattern (Gerber & Hopkins, 2011). Further analyses are needed to confirm this hypothesis but would be beyond the scope of the present study.

Heterochronic changes are better illustrated by the ontogenetic allometric trajectories of the two *Smutsia* species (Fig. 4; Supporting Information, Tables S6–S8), as they overlap in both size–shape and shape spaces (Supporting Information, Fig. S1; Mitteroecker *et al.*, 2005; Esquerré *et al.*, 2017). Both PC1 of the predicted values and multivariate regressions suggest that *S. temminckii* is paedomorphic, because it tends to resemble juvenile *S. gigantea* (peramorphic). Nevertheless, heterochrony is not always associated with close phylogenetic affinities. Differing ontogenetic allometric trajectories between closely related species were reported previously in hominids (Mitteroecker *et al.*, 2004). Despite being sister taxa, humans and chimpanzees differ in skull shape from early ontogenetic stages. The allometric trajectories of the two *Phataginus* species exhibit a similar pattern (Fig. 4; Supporting Information, Table S6). Both species show rather distinct intercepts (distinct shapes from early stages).

Overall, our results suggest that complex allometric changes played an important role in the morphological evolution of the pangolin skull. All pangolins follow a similar ontogenetic trend characterized by the elongation of the rostrum and a posterior projection of the zygomatic process of the maxilla (Figs 4, 5). As a consequence, the braincase is relatively smaller in larger species. These ontogenetic patterns are in line with described patterns of evolutionary allometry in which large-sized mammals evolve longer rostra (Cardini & Polly, 2013; Cardini *et al.*, 2015; Cardini, 2019). Our allometric and phenotypic trajectories (Fig. 4; Supporting Information, Fig. S2), associated with the thin plate spline deformations, enable us to suggest that the ontogenetic drift of *S. gigantea*

towards the Maninae (Asian pangolins) morphospace is attributable, in part, to the elongation of the skull associated with size (Fig. 5). Larger species with more elongated rostra (*Smutsia gigantea* and *Manis*) additionally present deep nasal notches (Supporting Information, Fig. S9).

Evolutionary patterns of ontogenetic allometry should therefore be taken into account in morphology-based studies. For instance, when looking at cranial character states in the morphology-based phylogeny from Gaudin *et al.* (2009), the depth of the nasal notch (character 306; Gaudin *et al.*, 2009) appears to be associated with size. The small-sized *Phataginus* species are the only ones presenting shallow nasal notches (Supporting Information, Fig. S9). The relative length of the parietal–squamosal suture (character 385; Gaudin *et al.*, 2009) also appears to be influenced by allometry (Figs 4, 5). The parietal–squamosal suture is relatively longer in skulls with shorter snouts, which is the case in *Phataginus* species (the smallest pangolins) that show a relatively long parietal–squamosal suture. This is to be expected, because skull length is influenced mostly by elongation of the rostrum in larger species (Figs 4, 5). According to Gaudin *et al.* (2009), *S. temminckii* is the only species presenting a multistate for this character [$< 25\%$ greatest skull length (0) or $> 25\%$ (1)], which is congruent with its short snout and intermediate average size between that of *Phataginus* spp. and that of *Manis* spp. and *S. gigantea* (Fig. 4). These results therefore call for a revision of some characters included in morphological matrices used to reconstruct extant and extinct pangolin phylogenetic relationships.

PATTERNS OF SKULL SHAPE VARIATION SUPPORT THE CLASSIFICATION OF EXTANT PANGOLINS IN THREE DISTINCT GENERA

Based on morphological features, pangolins have been classified from a single genus (*Manis*) to a maximum of six different genera. In 1882, Jentink published a monograph on the comparative anatomy of extant pangolins, except for *M. culionensis*, in which he briefly referred to the remarkable differences between the skulls of the seven recognized species (Jentink, 1882). Nevertheless, he ascribed all pangolin species to the same genus, postponing a thorough investigation of skull morphology. A division of pangolins into six different genera was later proposed by Pocock (1924), with the African *Smutsia* (*S. temminckii* and *S. gigantea*), *P. tricuspis*, *Uromanis longicaudata* (Linnaeus, 1766) (*P. tetradactyla*) and the Asian *M. pentadactyla*, *Paramanis javanica* and *Phatages crassicauda*. This classification was based on external/soft tissue characters only, but neglected cranial osteology.

Although the African–Asian split has been widely accepted, and the Asian genera have generally been merged into the single genus *Manis*, genus-level classifications have varied within the African clade. The four species have been ascribed either to a single genus, *Phataginus* (Patterson, 1978; Corbet & Hill, 1991), or kept separate in three distinct genera, as proposed by Pocock (1924; McKenna & Bell, 1997). Recent phylogenies based on morphological traits (Gaudin *et al.*, 2009) and molecular data (Gaubert *et al.*, 2018) have supported the view of an Asian–African split, with the Asian genus, *Manis* (Maninae), as the sister clade to the African pangolins composed of the two genera *Phataginus* (Phatagininae Gaubert, 2018) and *Smutsia* (Smutsiinae Gray, 1873).

Our results support the distinction of three extant pangolin genera, as recognized in previous works (Gaudin & Wible, 1999; Koenigswald, 1999; Gaudin *et al.*, 2009; Gaubert *et al.*, 2018). The PCAs and LDAs (Fig. 6A, B) largely reflect the division of extant Pholidota in Maninae (Asian; mostly positive PC1 values) and Smutsiinae + Phatagininae. The African clade was weakly supported in the most recent phylogeny based on anatomical characters (Gaudin *et al.*, 2009). In all analyses excluding fossil taxa, *Smutsia* spp. are recovered as a sister group to Maninae (Gaudin *et al.*, 2009). This might be explained, in part, by the detected allometric effect (see ‘Discussion: Size influences skull shape in extant pangolins’; Fig. 4; Supporting Information, Fig. S2). Nevertheless, both the PCA (Fig. 6B) and LDA (Fig. 6C, D) reveal the grouping of all *Manis* species to the exclusion of *Smutsia* and *Phataginus*. These analyses also show a clear separation between *Smutsia* and *Phataginus*, with the small pangolins showing lower values of PC1 and higher values of LD1.

We also show some degree of variation in skull shape at the intrageneric level that confirms species-level delineation of extant pholidotans (Fig. 6). Despite the split between *S. gigantea* and *S. temminckii* being slightly more recent than in other genera (5.6–13.2 Mya for *Smutsia*, 10.3–15.6 Mya for *Manis* and 9.3–16.5 Mya for *Phataginus*; Gaubert *et al.*, 2018), their skulls appear comparatively more distinct. Some of the differences between *S. temminckii* and *S. gigantea* are related to size (see above; Fig. 4). The most extensive morphological phylogenetic work performed to date found that *Smutsia* was the least-supported modern genus, with only three unique unambiguous synapomorphies, none of which involve the cranium (Gaudin *et al.*, 2009). Our results on variation in skull shape are congruent with the low support for the *Smutsia* node. As discussed above, elongation of the rostrum largely influences this intrageneric difference in shape. This allometric pattern is present at both ontogenetic and evolutionary levels and explains some

of the differences in skull shape between *S. gigantea* and *S. temminckii*. Although the shape of the skull of *S. gigantea* is more similar to that of Asian pangolins, *S. temminckii* is closer to *Phataginus* (Fig. 6). In addition to these substantial differences in skull shape within *Smutsia*, previous molecular analyses reported a relatively large mitogenomic distance within the genus (11.9%; Gaubert *et al.*, 2018), although lower than those reported within *Phataginus* (see below).

The two *Phataginus* species present the largest intrageneric mitogenomic distance (14.3%; Gaubert *et al.*, 2017). This distance is patent in PC3 and LD2 scores, which clearly separate *P. tetradactyla* from *P. tricuspis* (Fig. 6B, C). However, the cranial shape is more similar between the two *Phataginus* species than between the two *Smutsia* species (Supporting Information, Table S11). *Phataginus tetradactyla* was previously ascribed to the genus *Uromanis* (Pocock, 1924), but recent cladistic analyses based on osteological characters yielded a strong support for placement in the genus *Phataginus*, the best supported among all genera (Gaudin *et al.*, 2009). Of the seven unambiguous synapomorphies corresponding to cranial traits, the orientation and size of the zygomatic process of the squamosal (character 355; Gaudin *et al.*, 2009) is coded as ventrally directed and short dorsoventrally for both species of tree pangolin. We confirmed this character state (Fig. 6A; PC1), but additionally found that the shape of this process in the horizontal direction constitutes one of the main differences between the two species, with *P. tetradactyla* presenting the longest among all pholidotans (Fig. 6B; PC3).

Although three genera have been proposed in Maninae, recent studies have suggested that the three species should be grouped into the single genus, *Manis* (Gaudin *et al.*, 2009; Gaubert *et al.*, 2018). On average, *Manis* is the genus with the lowest (but still high) mitogenomic distance among species (mean = 9.3%), with *M. javanica*–*M. culionensis* showing the lowest value (3.1%) and *M. pentadactyla*–*M. javanica* / *M. culionensis* / *M. crassicaudata* showing the highest (12.2%; Gaubert *et al.*, 2017). The three species of Maninae show some overlap in morphospace, but are well segregated by PC2 (Fig. 6A). In contrast, *M. culionensis* overlaps with *M. javanica* in morphospace (Supporting Information, Fig. S1), which is congruent with the low mitogenomic distance and the recent divergence time estimated between these two species (0.4–2.5 Mya). However, our data are clearly insufficient to assess the morphological discrimination between *M. javanica* and *M. culionensis* (Supporting Information, Fig. S1).

Despite the strength of the Maninae node, infrageneric relationships have been greatly debated. Molecular-based analyses show a well-supported node (Bayesian posterior probability = 1), including

M. javanica/*M. culionensis* and *M. crassicaudata*, with *M. pentadactyla* as the sister taxon (Gaubert *et al.*, 2018). The *M. crassicaudata*–*M. javanica*/*M. culionensis* clade remains moderately supported in the Bayesian inference excluding mitogenomes (nuclear DNA only). In contrast, a moderately supported sister-group relationship between *M. pentadactyla* and *M. crassicaudata* is retrieved by morphology-based phylogenetic analyses (bootstrap value = 76; Gaudin *et al.*, 2009). The list of synapomorphies from Gaudin *et al.* (2009) for the node gathering *M. crassicaudata* and *M. pentadactyla* featured only three cranial traits. Among these, only the position of the foramen ovale at the level of the anterior edge of the ectotympanic is an unambiguous synapomorphy [character 379(1)]. Landmarks 18/43 and 20/45 describe this synapomorphy and contribute to segregate *M. crassicaudata* and *M. pentadactyla* from *M. javanica* along with other traits correlated with PC2 (Fig. 6A). Further anatomical investigation (i.e. internal characters) remains necessary to explore the morphological support for both hypotheses more thoroughly.

SKULL SHAPE VARIATION CORROBORATES CRYPTIC PHYLOGEOGRAPHICAL LINEAGES IN *P. TRICUSPIS*

Cranial osteological data are extremely useful to unveil patterns of cryptic speciation (Sukumaran & Knowles, 2017). Our results confirm, at least in part, the existence of several geographical groupings within *P. tricuspis* (Gaubert *et al.*, 2016, 2018; Figs 2, 7; Supporting Information, Fig. S5). The PCA showed some degree of overlap between the different lineages in morphospace (Fig. 7A, B), although we were able to find significant differences among the skulls of four lineages or lineage groups (Western Africa + Ghana, Dahomey Gap, Western Central Africa and Central Africa). Homogeneity in skull shape might be explained by recent divergence times between these lineages (0.8–4.6 Mya for the most recent common ancestor of Western and Central African lineages; Gaubert *et al.*, 2016, 2018). Nevertheless, we showed that two lineages (WAF and GHA) from a molecularly identified western lineage (DHG–GHA–WAF; Gaubert *et al.*, 2016) present a distinct cranial morphology (Figs 7C, D, 8). Furthermore, the Dahomey Gap lineage presents a distinct skull shape. Although the identification of group membership was not particularly high among cryptic lineages (75.4%), we showed that WAF–GHA, DHG and CAF–WCA form three morphologically distinct groups separated along a longitudinal gradient, with a high rate of a posteriori attributions (95.7%; Fig. 8).

Our results recover only partial evidence of the three nuclear groups found by Gaubert *et al.* (2016) that delineated Western Africa (WAF, GHA and DHG), Western Central Africa (WCA) and Central

Africa (CA). Although the grouping of WAF–GHA is congruent with the molecular phylogeny, the Dahomey Gap group is morphologically divergent in this clade. In addition, the similarity between Central Africa and Western Central Africa groups could suggest that they both retained a plesiomorphic cranial shape. However, testing the congruence between molecular and morphological data would require further scrutiny.

In contrast, we posit that different environmental conditions might also explain some parts of the cranial variation among pangolin lineages. The Dahomey Gap corresponds to a savannah-like corridor that divides western and central lowland rain forests (Dupont & Weinel, 1996), with a longitudinal gradient ranging from dry (Dahomey Gap) to more humid rainforest conditions (western and central rainforest). The adaptation to a drier climate resulting from tropical forest fragmentation (Salzmann & Hoelzmann, 2005) could explain the differentiation of a Dahomey Gap lineage. Concurrently, genetic drift resulting from an isolation-induced reduction of gene flow (Renaud & Millien, 2001) might also have played a role in the Dahomey Gap skull shape differentiation, following a vanishing refuge model of diversification (Vanzolini & Williams, 1981; Damasceno *et al.*, 2014; Gaubert *et al.*, 2016). At least three other endemic mammal species/subspecies have recently been described or confirmed on a genetic basis in the Dahomey Gap (Colyn *et al.*, 2010; Nicolas *et al.*, 2010; Hounghédji *et al.*, 2012). Further analyses are needed to assess the potential interaction between variation in skull shape and environmental conditions in pangolins.

INTRASPECIFIC VARIATION IN *M. JAVANICA*

In contrast to *P. tricuspis*, we did not find solid evidence of skull shape discrimination between molecularly identified lineages within *M. javanica*, because differences in shape appear to be associated solely with size (Supporting Information, Appendix S3; Figs S7, S8). The lack of differences in skull shape might be explained by introgressions between lineages or by more recent divergence times (Nash *et al.*, 2018) than among *P. tricuspis* lineages. Additionally, the cryptic lineages within *M. javanica* might currently lack a well-defined geographical delimitation, attributable, in part, to the lack of precise geographical information for the wild specimens sampled (Nash *et al.*, 2018). Human-induced specimen translocation by the introduction of pangolin seizures of unknown origin might also have resulted in the mixing of different lineages (Pantel & Chin, 2009).

CONCLUSION

Our results are congruent with the currently accepted genus- and species-level classification of extant

pangolins. We found that heterochronic changes explain, in part, the morphological differentiation of the skull at an intrageneric level. However, some species appear to present different allometric trajectories resulting from changes in skull shape during early developmental stages. Asian and African clades can be discriminated on the basis of the allometric trajectories of traits related to PC1. Namely, we identified elongation of the rostrum to be related to ontogenetic allometry, and we hypothesized that this might be also present at the evolutionary level. This might explain the detected differences in rostral proportions between species of different sizes and the apparent morphological convergence between *S. gigantea* and *Manis* species. Our results underline the importance of accounting for allometry when performing phylogenetic analyses based on morphological characters.

Our results also show that skull shape differs between cryptic lineages within *P. tricuspis*, and that these can be circumscribed into three geographical groups from western Africa (WAF–GHA), the Dahomey Gap (DHG) and Central Africa (CAF–WCA). We show that skull shape is potentially useful to determine pangolin species identity and, at a finer scale, the geographical origin of specimens of white-bellied pangolins seized in illegal trade hubs or markets. Such information could help to determine differential poaching pressures, delimitate management units, and thus refine threat status at a regional level.

ACKNOWLEDGEMENTS

We thank Steffen Bock, Frieder Mayer, Detlef Willborn (MfN), Roberto Portela Miguez, Louise Tomsett (BMNH), Géraldine Veron (MNHN), Chris Conroy (MVZ), Darrin Lunde, Paula Bohaska, John Ososky (USNM) and Eleanor Hoeger (AMNH) for access to collections. We acknowledge Farah Ahmed, Amin Garbout (BMNH) and Renaud Lebrun (ISEM) for assistance with micro-computed tomography scanning. We also thank Pierre-Henri Fabre, Quentin Martinez, and Julien Claude (ISEM) for fruitful discussions. Finally, we thank two anonymous reviewers for helpful comments on the manuscript. S.F.-C., L.H. and F.D. were supported by a European Research Council (ERC) consolidator grant (ConvergeAnt #683257). L.H. and F.D. were supported by Centre National de la Recherche Scientifique (CNRS). This research received support from the Synthesys Project, <https://www.synthesys.info/>, financed by the European Community Research Infrastructure Action under the FP7 (GB-TAF-5606 and BE-TAF-5661). This work was supported by PANGO-GO (ANR-17-CE02-0001) and by 'Investissements d'Avenir' grants managed by Agence Nationale de la Recherche Labex CEMEB

(ANR-10-LABX-0004), Labex NUMEV (ANR-10-LABX-0020). This is contribution ISEM 2019-150 of the Institut des Sciences de l'Évolution de Montpellier.

REFERENCES

- Adams DC, Collyer ML. 2009.** A general framework for the analysis of phenotypic trajectories in evolutionary studies. *Evolution* **63**: 1143–1154.
- Adams D, Collyer M, Kaliontzopoulou A, Sherratt E. 2017.** Geomorph: software for geometric morphometric analyses. R package, Version 3.0.5. Available at: <https://cran.r-project.org/package=geomorph>.
- Adams DC, Nistri A. 2010.** Ontogenetic convergence and evolution of foot morphology in European cave salamanders (Family: Plethodontidae). *BMC Evolutionary Biology* **10**: 216.
- Amrhein V, Greenland S, McShane B. 2019.** Scientists rise up against statistical significance. *Nature* **567**: 305–307.
- Bardin J, Rouget I, Cecca F. 2017.** Ontogenetic data analyzed as such in phylogenies. *Systematic Biology* **66**: 23–37.
- Benítez HA, Bravi R, Parra LE, Sanzana MJ, Sepúlveda-Zúñiga E. 2013.** Allometric and non-allometric patterns in sexual dimorphism discrimination of wing shape in *Ophion intricatus*: might two male morphotypes coexist? *Journal of Insect Science (Online)* **13**: 143.
- Bickford D, Lohman DJ, Sodhi NS, Ng PK, Meier R, Winker K, Ingram KK, Das I. 2007.** Cryptic species as a window on diversity and conservation. *Trends in Ecology & Evolution* **22**: 148–155.
- Cardini A. 2019.** Craniofacial allometry is a rule in evolutionary radiations of placentals. *Evolutionary Biology* **46**: 239–248.
- Cardini A, O'Higgins P. 2004.** Patterns of morphological evolution in *Marmota* (Rodentia, Sciuridae): geometric morphometrics of the cranium in the context of marmot phylogeny, ecology and conservation. *Biological Journal of the Linnean Society* **82**: 385–407.
- Cardini A, Polly PD. 2013.** Larger mammals have longer faces because of size-related constraints on skull form. *Nature Communications* **4**: 2458.
- Cardini A, Polly D, Dawson R, Milne N. 2015.** Why the long face? Kangaroos and wallabies follow the same 'rule' of cranial evolutionary allometry (CREA) as placentals. *Evolutionary Biology* **42**: 169–176.
- Challender DWS, Waterman C, Baillie JEM. 2014.** *Scaling up pangolin conservation. IUCN SSC Pangolin Specialist Group Conservation Action Plan*. London: Zoological Society of London.
- Cheverud JM. 1982.** Relationships among ontogenetic, static, and evolutionary allometry. *American Journal of Physical Anthropology* **59**: 139–149.
- Collyer ML, Adams DC. 2013.** Phenotypic trajectory analysis: comparison of shape change patterns in evolution and ecology. *Hystrix* **24**: 75–83.
- Colyn M, De Rennes U, Hulselmans J, Oude P. 2010.** Discovery of a new duiker species (Bovidae: Cephalophinae) from the Dahomey Gap, West Africa. *Zootaxa* **2637**: 1–30.

- Corbet GB, Hill JE. 1991. *A world list of mammalian species*. London: Natural History Museum Publishing and Oxford University Press.
- Damasceno R, Strangas ML, Carnaval AC, Rodrigues MT, Moritz C. 2014. Revisiting the vanishing refuge model of diversification. *Frontiers in Genetics* **5**: 353.
- Dryden IL, Mardia KV. 1993. Multivariate shape analysis. *Sankhyā: The Indian Journal of Statistics, Series A* **55**: 460–480.
- Dupont LM, Weinelt M. 1996. Vegetation history of the savanna corridor between the Guinean and the Congolian rain forest during the last 150,000 years. *Vegetation History and Archaeobotany* **5**: 273–292.
- Emry RJ. 1970. A North American Oligocene pangolin and other additions to the Pholidota. *Bulletin of the American Museum of Natural History* **142**: 455–510.
- Emry RJ. 2004. The edentulous skull of the North American pangolin, *Patriomanis americanus*. *Bulletin of the American Museum of Natural History* **285**: 130–138.
- Esquerré D, Sherratt E, Keogh JS. 2017. Evolution of extreme ontogenetic allometric diversity and heterochrony in pythons, a clade of giant and dwarf snakes. *Evolution* **71**: 2829–2844.
- Evin A, Cucchi T, Cardini A, Strand Vidarsdottir U, Larson G, Dobney K. 2013. The long and winding road: identifying pig domestication through molar size and shape. *Journal of Archaeological Science* **40**: 735–743.
- Ferreira-Cardoso S, Delsuc F, Hautier L. 2019. Evolutionary tinkering of the mandibular canal linked to convergent regression of teeth in placental mammals. *Current Biology* **29**: 468–475.e3.
- Foth C, Hedrick BP, Ezcurra MD. 2016. Cranial ontogenetic variation in early saurischians and the role of heterochrony in the diversification of predatory dinosaurs. *PeerJ* **4**: e1589.
- Galatius A, Kinze CC, Teilmann J. 2012. Population structure of harbour porpoises in the Baltic region: evidence of separation based on geometric morphometric comparisons. *Journal of the Marine Biological Association of the United Kingdom* **92**: 1669–1676.
- Gaubert P. 2011. Family Manidae. In: Wilson D, Mittermeier R, eds. *Handbook of the mammals of the world. Vol. 2. Hoofed mammals*. Barcelona: Lynx Edicions, 82–103.
- Gaubert P, Antunes A, Meng H, Miao L, Peigné S, Justy F, Njiokou F, Dufour S, Danquah E, Alahakoon J, Verheyen E, Stanley WT, O'Brien SJ, Johnson WE, Luo SJ. 2018. The complete phylogeny of pangolins: scaling up resources for the molecular tracing of the most trafficked mammals on earth. *The Journal of Heredity* **109**: 347–359.
- Gaubert P, Njiokou F, Ngua G, Afiademanyo K, Dufour S, Malekani J, Bi SG, Tougard C, Olayemi A, Danquah E, Djagoun CA, Kaleme P, Mololo CN, Stanley W, Luo SJ, Antunes A. 2016. Phylogeography of the heavily poached African common pangolin (Pholidota, *Manis tricuspis*) reveals six cryptic lineages as traceable signatures of Pleistocene diversification. *Molecular Ecology* **25**: 5975–5993.
- Gaudin TJ, Emry RJ, Wible JR. 2009. The phylogeny of living and extinct pangolins (Mammalia, Pholidota) and associated taxa: a morphology based analysis. *Journal of Mammalian Evolution* **16**: 235–305.
- Gaudin TJ, Gaubert P, Billet G, Hautier L, Ferreira-Cardoso S, Wible JR. 2019. Evolution & morphology. In: Challender DWS, Nash H, Waterman C, eds. *Pangolins: science, society and conservation*. Cambridge: Academic Press.
- Gaudin TJ, Wible JR. 1999. The entotympanic of pangolins and the phylogeny of the Pholidota (Mammalia). *Journal of Mammalian Evolution* **6**: 39–65.
- Gerber S, Hopkins MJ. 2011. Mosaic heterochrony and evolutionary modularity: the trilobite genus *Zacanthopsis* as a case study. *Evolution* **65**: 3241–3252.
- Goswami A. 2006. Cranial modularity shifts during mammalian evolution. *The American Naturalist* **168**: 270–280.
- Gray JA, Sherratt E, Hutchinson MN, Jones MEH. 2019. Changes in ontogenetic patterns facilitate diversification in skull shape of Australian agamid lizards. *BMC Evolutionary Biology* **19**: 7.
- Gunz P, Mitteroecker P, Neubauer S, Weber GW, Bookstein FL. 2009. Principles for the virtual reconstruction of hominin crania. *Journal of Human Evolution* **57**: 48–62.
- Hatt RT, Lang H, Chapin JP. 1934. The pangolins and aardvarks collected by the American Museum Congo Expedition. *Bulletin of the American Museum of Natural History* **66**: 643–672.
- Hautier L, Billet G, Eastwood B, Lane J. 2014. Patterns of morphological variation of extant sloth skulls and their implication for future conservation efforts. *The Anatomical Record* **297**: 979–1008.
- Hautier L, Billet G, de Thoisy B, Delsuc F. 2017. Beyond the carapace: skull shape variation and morphological systematics of long-nosed armadillos (genus *Dasyops*). *PeerJ* **5**: e3650.
- Hebert PDN, Penton EH, Burns JM, Janzen DH, Hallwachs W. 2004. Species realities and numbers in sexual vertebrates: perspectives from an asexually transmitted genome. *Proceedings of the National Academy of Sciences of the United States of America* **96**: 992–995.
- von Helversen O, Heller KG, Mayer F, Nemeth A, Volleth M, Gombkötö P. 2001. Cryptic mammalian species: a new species of whiskered bat (*Myotis alcaethoe* n. sp.) in Europe. *Die Naturwissenschaften* **88**: 217–223.
- Houngbédji MG, Djossa BA, Adomou AC, Dakpogan SC, Sinsin B, Mensah GA. 2012. Conservation status of the red-bellied guenon (*Cercopithecus erythrogaster erythrogaster*) in the western Dahomey Gap in southwestern Benin and the adjacent Togodo Forest Reserve, south Togo. *African Primates* **7**: 184–192.
- Jentink FA. 1882. Revision of the Manidae in the Leyden Museum. *Notes from the Leyden Museum* **4**: 193–209.
- Klingenberg CP. 2011. MorphoJ: an integrated software package for geometric morphometrics. *Molecular Ecology Resources* **11**: 353–357.
- Klingenberg CP. 2013. Cranial integration and modularity: insights into evolution and development from morphometric data. *Hystrix* **24**: 43–58.
- Klingenberg CP. 2016. Size, shape, and form: concepts of allometry in geometric morphometrics. *Development Genes and Evolution* **226**: 113–137.

- McKenna MC, Bell SK. 1997.** *Classification of mammals above the species level*. New York: Columbia University Press.
- Miranda FR, Casali DM, Perini FA, Machado FA, Santos FR. 2018.** Taxonomic review of the genus *Cyclopes* Gray, 1821 (Xenarthra: Pilosa), with the revalidation and description of new species. *Zoological Journal of the Linnean Society* **183**: 687–721.
- Mitteroecker P, Gunz P, Bernhard M, Schaefer K, Bookstein FL. 2004.** Comparison of cranial ontogenetic trajectories among great apes and humans. *Journal of Human Evolution* **46**: 679–697.
- Mitteroecker P, Gunz P, Bookstein FL. 2005.** Heterochrony and geometric morphometrics: a comparison of cranial growth in *Pan paniscus* versus *Pan troglodytes*. *Evolution & Development* **7**: 244–258.
- Moraes-Barros N, Miyaki CY, Morgante JS. 2007.** Identifying management units in non-endangered species: the example of the sloth *Bradypus variegatus* Schinz, 1825. *Brazilian Journal of Biology* **64**: 829–837.
- Murphy W, Eizirik E, Johnson W, Zhang Y. 2001a.** Molecular phylogenetics and the origins of placental mammals. *Nature* **409**: 614–618.
- Murphy W, Eizirik E, O'Brien S, Madsen O, Scally M, Douady C, Teeling E, Ryder O, Stanhope M, De Jong W, Springer M. 2001b.** Resolution of the early placental mammal radiation using Bayesian phylogenetics. *Science* **294**: 2348–2351.
- Nash HC, Low GW, Choo SW, Chong JL, Semiadi G, Hari R, Sulaiman MH, Turvey TS, Evans TA, Rheindt FE. 2018.** Conservation genomics reveals possible illegal trade routes and admixture across pangolin lineages in Southeast Asia. *Conservation Genetics* **19**: 1083–1095.
- Nicolas V, Olayemi A, Wendelen W, Colyn M. 2010.** Mitochondrial DNA and morphometrical identification of a new species of *Hylomyscus* (Rodentia: Muridae) from West Africa. *Zootaxa* **2579**: 30–44.
- Pantel S, Chin SY. 2009.** *Proceedings of the workshop on trade and conservation of pangolins native to South and Southeast Asia*. Singapore: TRAFFIC Southeast Asia.
- Patterson B. 1978.** Pholidota and Tubulidentata. In: Maglio VJ, Cooke HBS, eds. *Evolution of African Mammals*. Cambridge: Harvard University Press, 268–278.
- Piras P, Salvi D, Ferrara G, Maiorino L, Delfino M, Pedde L, Kotsakis T. 2011.** The role of post-natal ontogeny in the evolution of phenotypic diversity in *Podarcis* lizards. *Journal of Evolutionary Biology* **24**: 2705–2720.
- Pocock RI. 1924.** The external characters of the pangolins (Manidae). *Proceedings of the Zoological Society of London* **94**: 707–723.
- R Development Core Team. 2013.** *R: a language and environment for statistical computing*.
- Renaud S, Millien V. 2001.** Intra- and interspecific morphological variation in the field mouse species *Apodemus argenteus* and *A. speciosus* in the Japanese archipelago: the role of insular isolation and biogeographic gradients. *Biological Journal of the Linnean Society* **74**: 557–569.
- Rohlf F, Slice D. 1999.** Extensions of the Procrustes method for the optimal superimposition of landmarks. *Systematic Biology* **39**: 40–59.
- Salzmann U, Hoelzmann P. 2005.** The Dahomey Gap: an abrupt climatically induced rain forest fragmentation in West Africa during the late Holocene. *The Holocene* **15**: 190–199.
- Schlager S. 2017.** Morpho and Rvcg – shape analysis in R. In: Zheng G, Li S, Székely G, eds. *Statistical shape and deformation analysis*. London: Academic Press, 217–256.
- Sidlauskas B, Mol J, Vari R. 2011.** Dealing with allometry in linear and geometric morphometrics: a taxonomic case study in the *Leporinus cylindriciformis* group (Characiformes: Anostomidae) with description of a new species from Suriname. *Zoological Journal of the Linnean Society* **162**: 103–130.
- Sukumaran J, Knowles LL. 2017.** Multispecies coalescent delimits structure, not species. *Proceedings of the National Academy of Sciences of the United States of America* **114**: 1607–1612.
- Sveegaard S, Galatius A, Dietz R, Kyhn L, Koblitz JC, Amundin M, Nabe-Nielsen J, Sinding MHS, Andersen LW, Teilmann J. 2015.** Defining management units for cetaceans by combining genetics, morphology, acoustics and satellite tracking. *Global Ecology and Conservation* **3**: 839–850.
- Vanzolini P, Williams E. 1981.** The vanishing refuge: a mechanism for ecogeographic speciation. *Papéis Avulsos de Zoologia* **34**: 251–255.
- Venables WN, Ripley BD. 2002.** *Modern applied statistics with S*. New York: Springer.
- Villemant C, Simbolotti G, Kenis M. 2007.** Discrimination of *Eubazus* (Hymenoptera, Braconidae) sibling species using geometric morphometrics analysis of wing venation. *Systematic Entomology* **32**: 625–634.
- Voje KL, Hansen TF, Egset CK, Bolstad GH, Pélabon C. 2014.** Allometric constraints and the evolution of allometry. *Evolution* **68**: 866–885.
- Von Koenigswald W. 1999.** Order Pholidota. In: Rössner G, Heissig K, eds. *The Miocene land mammals of Europe*. Munich: Dr Friedrich Pfeil, 75–80.
- Zhang H, Miller M, Yang F, Chan HK, Gaubert P, Ades G, Fischer GA. 2015.** Molecular tracing of confiscated pangolin scales for conservation and illegal trade monitoring in Southeast Asia. *Global Ecology and Conservation* **4**: 414–422.
- Zhou ZM, Zhou Y, Newman C, Macdonald DW. 2014.** Scaling up pangolin protection in China. *Frontiers in Ecology and the Environment* **12**: 97–98.

SUPPORTING INFORMATION

Additional supporting information may be found in the online version of this article at the publisher's web-site:

Appendix S1. Specimen list and landmark coordinates.

Appendix S2. Discrete traits.

Appendix S3. Additional analyses.

Appendix S4. LDA a posteriori attribution tables.

Table S1. Definitions of the 75 cranial landmarks used.

Table S2. Phylogenetic ANOVA of shape (Procrustes coordinates) ~ log(centroid size). *Significant *P*-value. The randomized residual permutation procedure used 10 000 permutations.

Table S3. Pairwise comparisons of the allometric trajectory angles for skull shape. *P*-values (10.000 iterations) are in the upper triangle and angles between slopes (in degrees) in the lower triangle. Significant results are written in bold.

Table S4. Pairwise comparisons of the phenotypic trajectory angles. *P*-values (10 000 iterations) are in the upper triangle and angles between path distances in the lower triangle. Significant results are written in bold.

Table S5. Pairwise comparisons of the phenotypic trajectory lengths. *P*-values (10 000 iterations) are in the upper triangle and absolute differences between path distances in the lower triangle. Significant results are written in bold.

Table S6. Pairwise comparison of the intercept ($x = 5.125$) of the multivariate Procrustes allometric regressions (overlap test). *P*-values (Hochberg corrected) of the difference between the intercepts computed with 10 000 iterations are in the upper triangle and observed differences in the lower triangle. Taxa with significantly non-parallel trajectories were not included in the test. Significant results are written in bold.

Table S7. Pairwise comparison of the intercept ($x = 0$) of the multivariate Procrustes allometric regressions (overlap test). *P*-values of the difference between the intercepts computed with 10 000 iterations are in the upper triangle and observed differences in the lower triangle. Taxa with significantly non-parallel trajectories were not included in the test. Significant results are written in bold.

Table S8. Pairwise comparisons of the predicted head shape (predicted Procrustes residuals) differences at maximum centroid size (heterochrony test). *P*-values (Hochberg corrected; in black for $x = 5.125$ and in blue for $x = 0$) of the difference between them computed with 10 000 iterations are in the upper triangle and observed differences in the lower triangle. Taxa with significantly non-parallel trajectories were not included in the test. Significant results are written in bold.

Table S9. Pairwise comparison of the principal component 1 (PC1) allometric trajectory intercepts for skull shape. *P*-values of a multiple comparison of means (Tukey's test) are in the upper triangle and the *t*-statistics values in the lower triangle. The same intercept in all species is the null hypothesis. The *P*-values are indicated for species that show the same intercept; *all other pairwise comparisons retrieved a *P*-value < 0.001. Only species with parallel slopes are included. Significant results are written in bold.

Table S10. ANOVA of shape (Procrustes coordinates) ~ sex*species and shape (Procrustes coordinates) ~ size + sex*species. *Significant *P*-value. The randomized residual permutation procedure used 10 000 permutations.

Table S11. Pairwise comparison of the Procrustes distances between least-squares (LS) means for species. *P*-values of the difference between the LS means computed with 10 000 iterations are in the upper triangle and observed distances in the lower triangle. Significant results are written in bold.

Table S12. ANOVA of shape ~ taxa/geographical groups of adult specimens of the interspecific, *Phataginus tricuspis* and *Manis javanica* datasets. Significant *P*-values indicate differences between skull shapes of taxa/geographical groups; *n* groups is the number of taxa or geographical groups used as factors. *Significant *P*-value. The randomized residual permutation procedure used 10 000 permutations.

Table S13. Pairwise comparison of the allometry-corrected Procrustes distances between least-squares (LS) means for species. *P*-values of the difference between the LS means computed with 10 000 iterations are in the upper triangle and observed distances in the lower triangle. Significant results are written in bold.

Table S14. Significant *t*-tests of principal components vs. log-transformed centroid size.

Table S15. Pairwise comparisons of the allometric trajectory angles for skull shape in *Phataginus tricuspis* cryptic lineages [homogeneity of slopes (HOS)]. *P*-values (10 000 iterations) are in the upper triangle and angles between slopes (in degrees) in the lower triangle. Significant results are written in bold.

Table S16. Pairwise comparison of the Procrustes distances between least-squares (LS) means for cryptic lineages (Gaubert *et al.*, 2016). *P*-values of the difference between the LS means computed with 10 000 iterations are in the upper triangle and observed distances in the lower triangle. Significant results are written in bold.

Table S17. Pairwise comparison of the Procrustes distances between least-squares (LS) means for three geographical groups. *P*-values of the difference between the LS means computed with 10 000 iterations are in the upper triangle and observed distances in the lower triangle. Significant results are written in bold.

Table S18. Pairwise comparison of the allometry-corrected Procrustes distances between least-squares (LS) means for cryptic lineages (Gaubert *et al.*, 2016). *P*-values of the difference between the LS means computed with

10 000 iterations are in the upper triangle and observed distances in the lower triangle. Significant results are written in bold.

Table S19. Pairwise comparison of the allometry-corrected Procrustes distances between least-squares (LS) means for three geographical groups. *P*-values of the difference between the LS means computed with 10 000 iterations are in the upper triangle and observed distances in the lower triangle. Significant results are written in bold.

Table S20. ANOVA of shape (Procrustes coordinates) ~ log(centroid size)*cryptic lineages (*N* = 35) in *M. javanica*. *Significant *P*-value.

Figure S1. Principal components analysis on the dataset including juveniles and two specimens of *Manis culionensis* (*N* = 243).

Figure S2. Phenotypic trajectory analysis among seven pangolin species. The morphospace delimited by principal component (PC)1 and PC2 explaining the variance between adults and juveniles within each species (*N* = 125) is shown. For each species, a trajectory representing the change in shape between the shape estimates for juveniles (light grey circles) and adults (dark grey circles) is represented. Deformed meshes represent the maximum and minimum shapes of PC1 and PC2.

Figure S3. Principal component (A, PC1 vs. PC2; B, PC1 vs. PC3) and linear discriminant analyses (C, LD1 vs. LD2; D, LD1 vs. LD3), with associated allometry-corrected variation in shape, for crania of seven pangolin species (*N* = 173). Shapes are the residuals of a pooled within-group multivariate regression of shape on log-transformed centroid size.

Figure S4. Allometric trajectories of the cryptic lineages (Gaubert *et al.*, 2016) of *Phataginus tricuspis* (*N* = 95). The *x*-axis values are the log-transformed centroid sizes for each specimen; the *y*-axis values are the principal component 1 of the predicted values of multivariate regression of shape ratios on size. The size of the dots indicates the size of the specimens. Abbreviation: CAF, Central Africa; DHG, Dahomey Gap; GHA, Ghana; WAF, Western Africa; WCA, Western Central Africa. GAB (Gabon) was excluded because our dataset included only one skull.

Figure S5. Mean shapes of proposed management units for the *Phataginus tricuspis* sample (*N* = 70) in lateral (left), ventral (middle) and dorsal (right) views. A, Central African region. B, Dahomey Gap region. C, Western African region. Black dots are landmark positions.

Figure S6. Principal components (A, PCres1 vs. PCres2; B, PCresC1 vs. PCres3) and linear discriminant analyses (C, LD1 vs. LD2; D, LD1 vs. LD3) with associated allometry-corrected variation in shape for crania of six cryptic lineages of *Phataginus tricuspis* (*N* = 71; Gaubert *et al.*, 2016). Shapes are the residuals of a pooled within-group multivariate regression of shape on log-transformed centroid size.

Figure S7. Allometric trajectories of the lineages (Nash *et al.*, 2018) of *Manis javanica* (*N* = 35). The *x*-axis values are the log-transformed centroid sizes for each specimen; *y*-axis values are the principal component 1 of the predicted values of multivariate regression of shape ratios on size. The size of the dots indicates the size of the specimens. Abbreviations: BOR, Borneo; JAV, Java; SUM/SIN, Sumatra/Singapore.

Figure S8. Principal components (A, PC1 vs. PC2; B, PC1 vs. PC3) with associated variation in shape for crania of *Manis javanica* lineages (*N* = 25; Nash *et al.*, 2018).

Figure S9. Minimum (left) and maximum (right) shape prediction from a multivariate regression on log-transformed centroid size for two species of small (A, B) and two species of large (C, D) pangolins in dorsal view. A, *Phataginus tricuspis*. B, *Phataginus tetradactyla*. C, *Smutsia gigantea*. D, *Manis javanica*. Grey and red dots mark landmark positions at minimum and maximum sizes, respectively. Black dots are landmark positions for maximum size predictions.